GEOMETRIC MODELING AND ANALYSIS OF ROD-LIKE LARGE SPACE STRUCTURES*

by

A. H. Nayfeh
M. S. Hefzy

Department of Aerospace Engineering and Applied Mechanics
University of Cincinnati, Cincinnati, Ohio 45221

ABSTRACT

The application of geometrical schemes similar to those of Buckminster Fuller's geodesic dome to large sphere antenna reflectors has been investigated. The purpose of these studies is to determine the shape and size of flat segmented surfaces which approximate general shells of revolution and in particular spherical and paraboloidal reflective surfaces. The extensive mathematical and computational geometry analyses of the reflector have resulted in the development of a general purpose computer program. This program is capable of generating the complete design parameters of the dish and can meet stringent accuracy requirements. The computer program also includes a graphical "self contained" subroutine which enables one to graphically display the required design.

(NASA-CR-158509) GEOMETRIC MODEL AND ANALYSIS OF ROD-LIKE LARGE SPACE STRUCTURES (Cincinnati Univ.) 64 p HC A04/MF A01 CSCI 22B

N79-23128

Unclas
G3/15 25157

* Research supported by NASA Grant NSG 1185. The authors would like to thank M. Anderson, H. Bush, M. Card and M. Mikulas of NASA Langley for many helpful discussions throughout the development of this work.

I. INTRODUCTION

The last decade has witnessed a dramatic increase in the research activities dealing with the possibility of utilizing space for various commercial and scientific needs. In several recent issues of Astronautics and Aeronautics (see, for example, [1-4]), many articles have appeared which deal with diverse aspects of large space structures. These articles have identified various applications and also proposed novel designs of structures to meet such applications. A review of the research activities on space structures prior to 1966 has been documented in volume [5] that resulted from an International Conference on space structures.

It has thus become necessary to find and analyze small lightweight structures that will be used easily to construct much larger space structures. It would be desirable for these structures to be isotropic in nature. However, construction requirements may make this infeasible, therefore requiring orthotropic or possibly completely anisotropic structures. The latter is also undesirable because of the added complexity to the problem. Truss-type periodic (repetitive) structures have recently been analyzed as candidates for space structures [5-8]. Here simplicity in construction coupled with large stiffness to density ratios will be most desirable. However, up to now, most of the extensive modeling and design of rod-like space structures have been concerned with flat structures in the form of either plates or three-dimensional Cartesian structures [7-9].

Rod-like structures in the form of spherical domes have previously been modeled and analyzed as candidates for many on-ground structural applications. These are known as the geodesic domes and constitute variations on the original spherical dome invented by Buckminster Fuller [10,11].

The flat rod-like models studied so far in [7-9] are restricted in their possible applications to such structures as floors, ceilings and straight walls. However, the results reported in [7-9], although presented an initial stage in the understanding of the behavior of large space structures, gave insight and confidence into the possible extension to the study of more geometrically complicated structures. Shallow shell structures have frequently been mentioned, for example, as candidates for building components in communication systems, orbiting antenna, and solar energy satellites.

In this report we describe methods of designing and estimating the geometric accuracy of rod-like shells of revolutions. These will consist of single surface shells in the form of either spherical or paraboloidal shells. Although our analysis will be kept general we do this with an important application in mind; namely the design and geometric analysis of large space antennas.

Our ambitious aim of modeling general rod-like shallow shells of revolutions cannot be achieved in one shot and thus has to wait until we develop further basic understanding of some simplified special cases. Here we conceive of the general shell to also include the cases of concentric shells with rod-like internal and external surfaces and cores. Having analyzed the flat rod-like structures the immediate difficulty in the study of the corresponding curved structures lies in the modeling (specification) of their geometry. In the case of the flat structures the geometric arrangement is practically trivial since most of them can be constructed by using only a few number of different length columns. As an example, we recall that the tetrahedral model of [7] and the octetruss model of [9] use single rod length elements.

II. LITERATURE REVIEW OF SPHERICAL GEODESIC DOMES

General Description:

The transition from a flat rod-like surface to its corresponding curved surface introduces tremendous amounts of geometric difficulties and constraints. Consider for example, the case of a $(0, \pm 60^{\circ})$ flat plate arrangement shown in figure 1. Here all rods have the same length. Now, in trying to deform figure 1 to fit on a spherical surface for example, one finds it impossible to do so, especially if he insists on maintaining the lengths of the members to stay the same. In so trying one soon realizes that he does not have enough mathematical tools to construct such a discrete spherical shell. The geometric constraints encountered in constructing rod-like shells can only be understood and utilized if one familiarizes himself with the appropriate mathematical tools such as geodesics. Here geodesics is defined as the technique for constructing shell-like structures that hold themselves up without supporting columns. They could be very light and very strong. They can also be very large and hence attractive for space as well as earth structures. The geodesic spherical bubble erected to house the United States exhibits at EXPO '67 in Montreal is an example which exhibits all of the above attractive properties. Smaller geodesic domes have also been used as cabins, offices, playgrounds, and pavillians, etc. Yet, considering their apparent potential, in the quarter-century since Buckminster Fuller introduced them they have not been used very widely. This is perhaps due to the fact that they are mathematically derived structures and their mathematics has not been easily available. Parts for the self-supporting frame must be fabricated to close specification. The fabrication, with today's technology, is no problem, the problem is learning what the specifications should be.

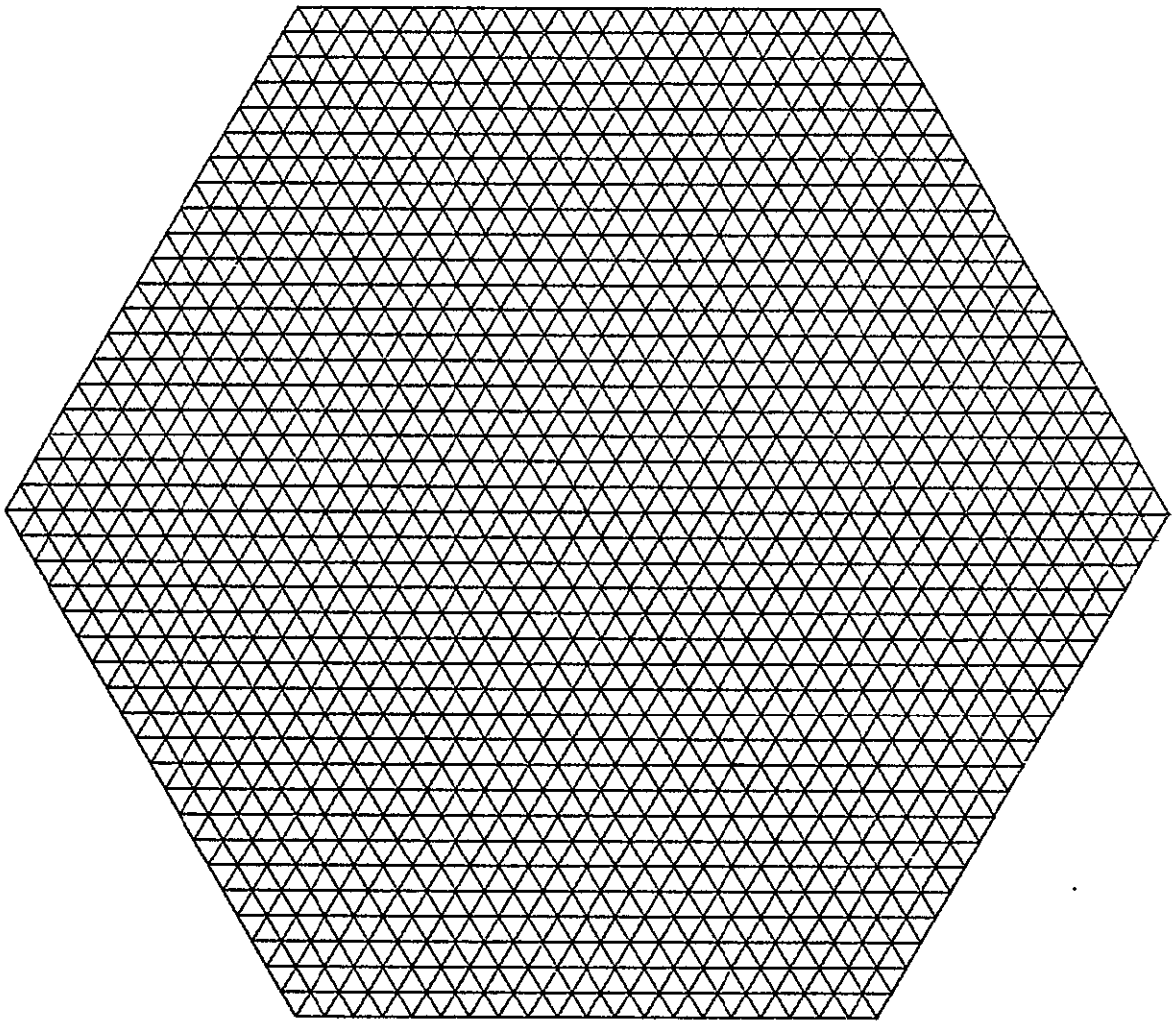

FIG. 1. $(0^{\circ}, \pm 60^{\circ})$ ARRAY

In developing the geodesic dome, Fuller recognized that the equilateral triangle was the most basic geometric structure which is also inherently very stable and strong. By translating, rotating and piecing these triangles together one can form regular polyhedra. One specific polyhedron, the icosahedron, was found to best approximate the sphere of all other polyhedronal forms.

To see how this works, consider the twenty identical equilateral triangles of figure 2a. By cutting along the outer sides of this figure, wrapping it around and connecting the edges one gets the icosahedron of figure 2b. This icosahedron will have twenty identical triangular faces, twelve vertices and thirty equal lengthed edges. Moreover, there exists a unique sphere which circumscribes this icosahedron and passes through its twelve vertices. If one imagines blowing up the icosahedron to completely fill the sphere one recognizes that the twelve vertices maintain their original positions but the triangular sides become spherical and lie on the sphere. From the above discussions we can conclude that the icosahedron constitutes a rather rough approximation of a sphere. Better approximations can be obtained, however, by subdividing the individual icosahedron triangles into smaller ones and blowing them up to locate their vertices on the sphere. These subdivisions are known as the frequencies of the structure. The higher the frequency, the closer one gets to the sphere. Upon further subdivisions, one soon realizes, however, that the geometric constraints become enormous (as will be shown later, for example, the number of different lengths is roughly in the order of the square of the frequency). Various methods of subdividing the icosa triangles have been reported in the literature (see, for examples [10,11]).

Simple geometric consideration will reveal that the side length L of the icosahedron is equal to 1.051462R where R is the radius of the sphere circumscribing it. For further discussion of the spherical geodesic dome descriptions

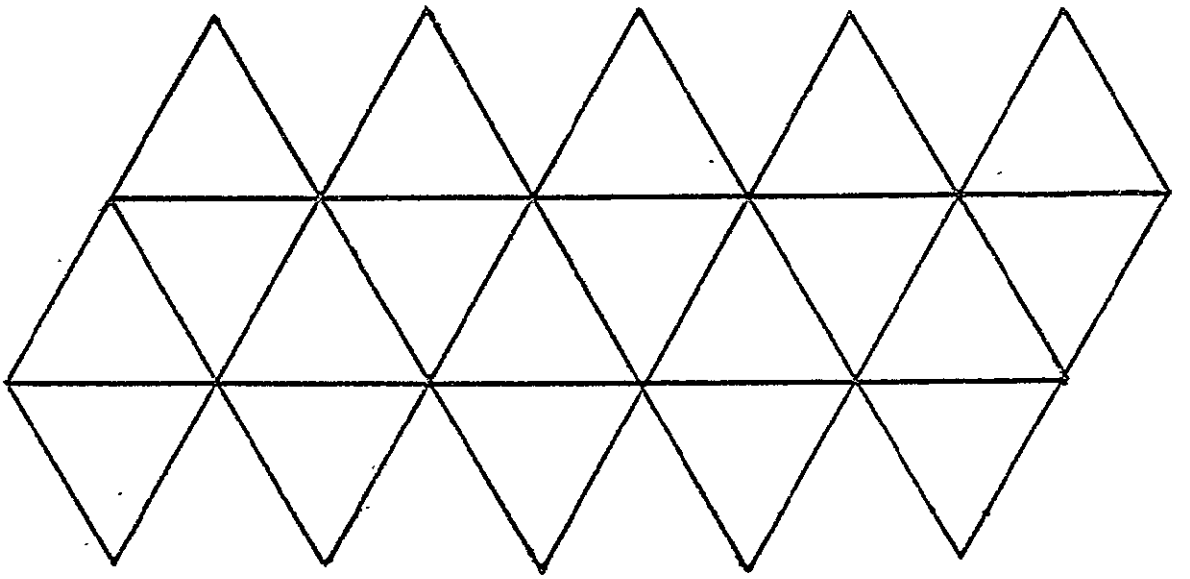

FIG. 2a. ICOSA TRIANGLES

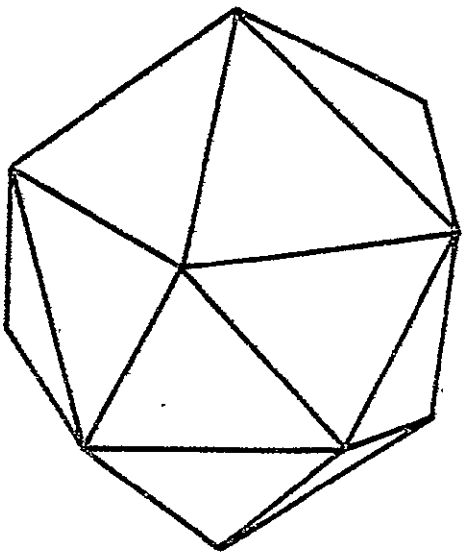

FIG. 2b. ICOSAHEDRON

we refer the reader to [10,11]. In what follows however, we shall treat the geodesic spherical dome as a very special case of our intended general modeling of rod-like spherical and paraboloidal caps.

Having identified large space shallow antennas as important application of our rod-like shells we here point out the insufficiency and the inflexibility of the Fuller type geodesic spherical dome to meet their general geometric requirement. For one thing in trying to extract a complete cap of the Fuller sphere it will be found out that such a cap will have a unique focus to aperture diameter ratio (referred to as FOD). Thus arbitrary degrees of cap shallowness will not be possible to model. Secondly, the number of rods emanating from the various vertices of the subdivision triangles (once on the sphere) will not be uniform. Specifically from each of the original twelve icosahedron vertices there emanate five rods where as from all the remaining subdivision vertices there emanate six rods. This nonuniformity will influence the degree of smoothness required. Thirdly, in constructing the Fuller sphere only the center of the sphere is used as the projection center of the subdivisions. Fourthly, further development and analysis will be required to construct a Fuller type paraboloidal shell. The above unattractive properties of the Fuller shell will be more obvious later on in our modeling analysis once we introduce the many nonrestrictive geometric degrees of freedom.

III. ANTENNAS IN THE FORM OF ROD-LIKE SHELLS OF REVOLUTION

In order to use rod-like structures as good candidates for building large space antennas we must first understand the global geometric description of the required structure. Specifically we must know if the antenna will be a part of a sphere, parabolid, ellipsoid or any other form of shells of revolutions. Once this is specified, two extra parameters* such as the height, H and the aperture radius, R_1, of the shell cup will be enough to completely specify the required geometry.

A typical shallow shell of revolution cap is shown in figure 3a. By changing the ratio of H to R_1 various degrees of shallowness will be realized. As for the rod-like approximation of the cap we proceed as follows: We subdivide the circumference of the aperture circle into n identical segments where n is an arbitrary integer. The points connecting these segments are numbered 2 - (n+1) and are then connected with the vertix point 1 (as shown for example in figure 3b for n=8) to form an n identical sided pyramid. In terms of H and R_1, the side lengths of the individual triangular face of the pyramid are given by

$$L_1 = (R_1^2 + H^2)^{1/2} \tag{1}$$

$$L_2 = 2R_1 \sin \frac{\pi}{n} \tag{2}$$

This pyramid will then form the roughest discrete approximation of the cap. Better approximations can be obtained, however, by subdividing the individual original pyramid triangular faces into smaller triangles and blowing them up to locate their vertices on the desired solid surface (see Figures 4-6 for procedure illustration). These subdivisions are

---

* If R_1 and FOD are the given two parameters then H can be calculated as $H = 2\ \text{FOD} \times R_1\left[1 - \left\{1 - \frac{1}{16(\text{FOD})^2}\right\}^{1/2}\right]$ for a sphere and $H = R_1/(16\ \text{FOD})$ for a paraboloid.

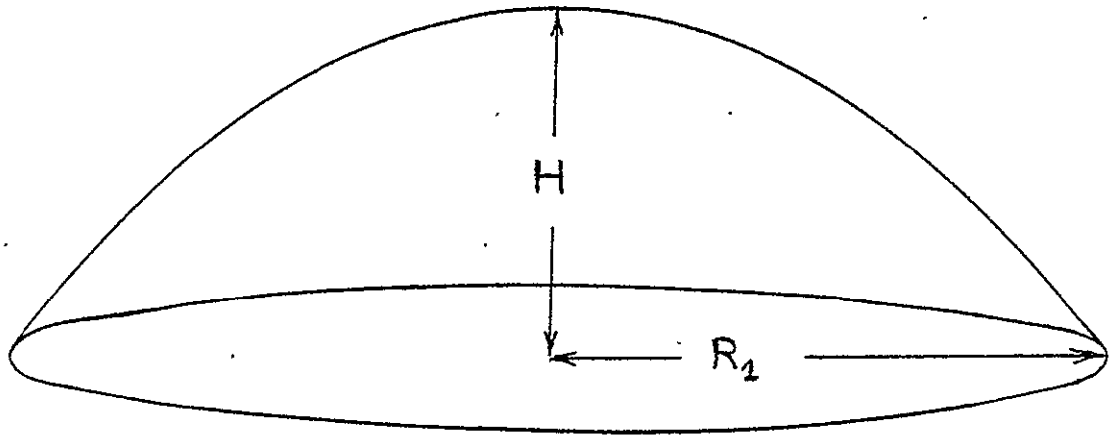

FIG. 3a. REPRESENTATIVE DISH

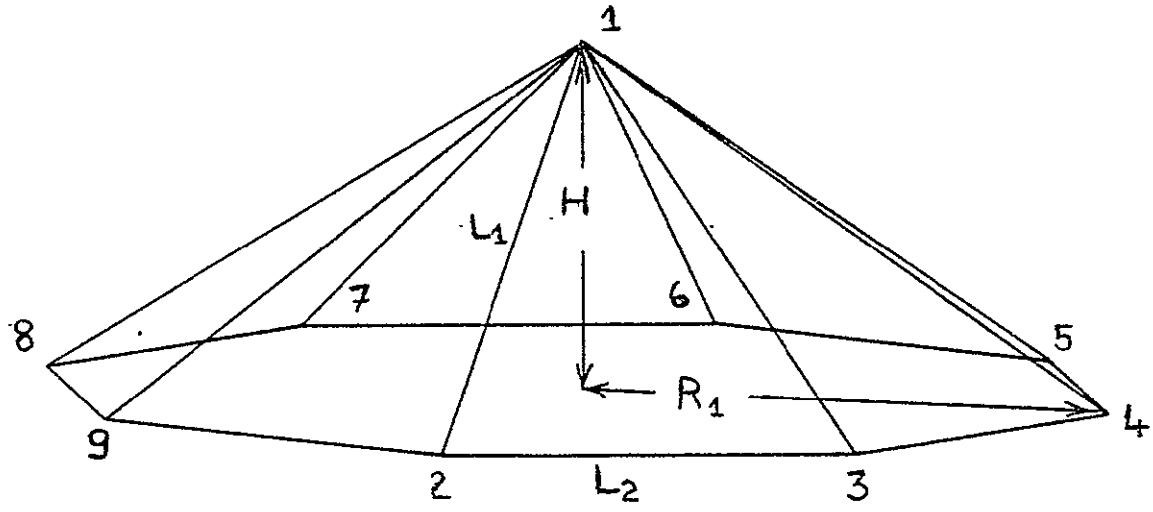

FIG. 3b. PYRAMID APPROXIMATION (n=8)

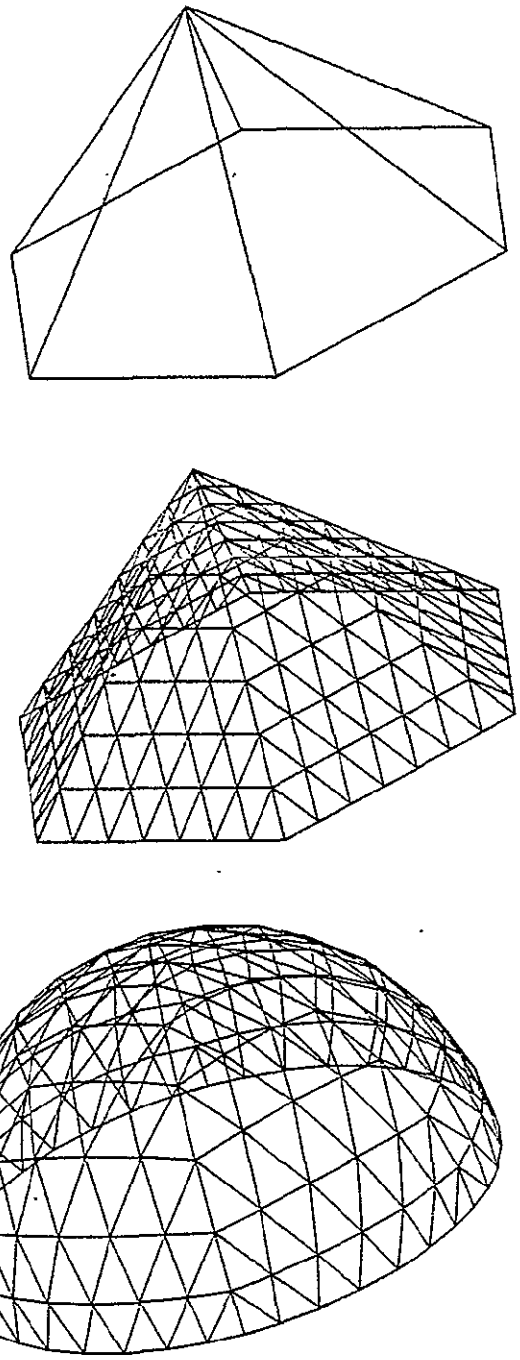

FIG. 4. PROCEDURE ILLUSTRATION OF SUBDIVISION AND BLOWING (n=6, N=7, FOD = 0.25)

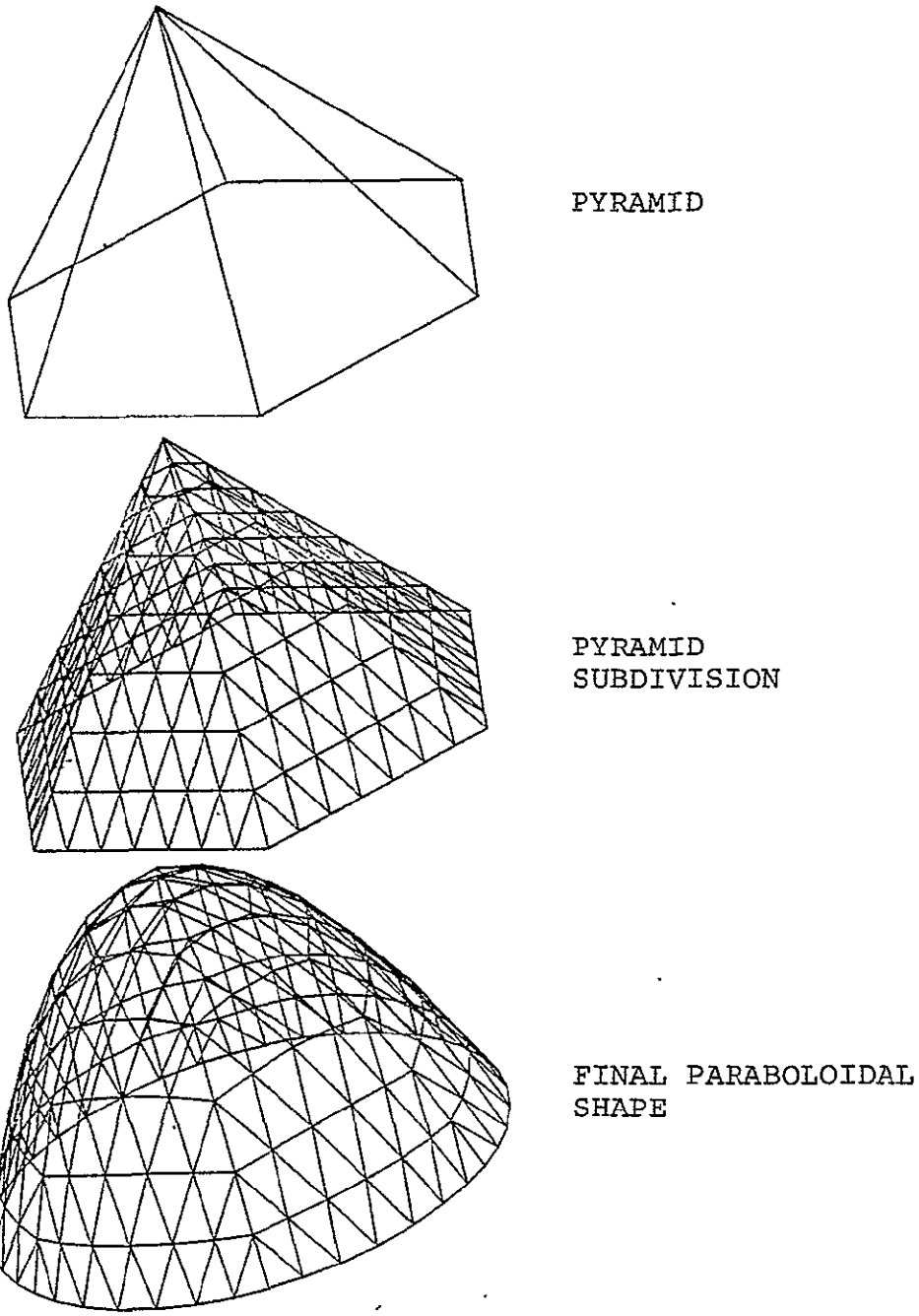

FIG. 5. PROCEDURE ILLUSTRATION OF SUBDIVISION AND BLOWING (n=6, N=7, FOD = 0.25)

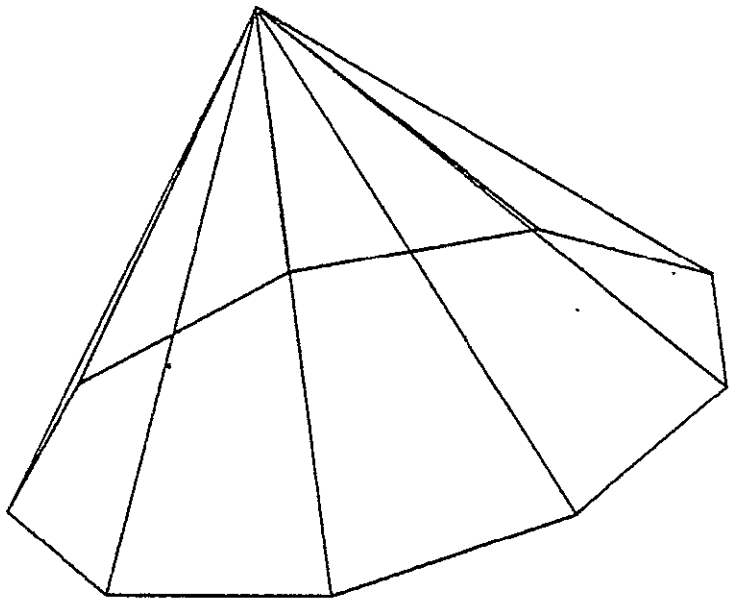

PYRAMID

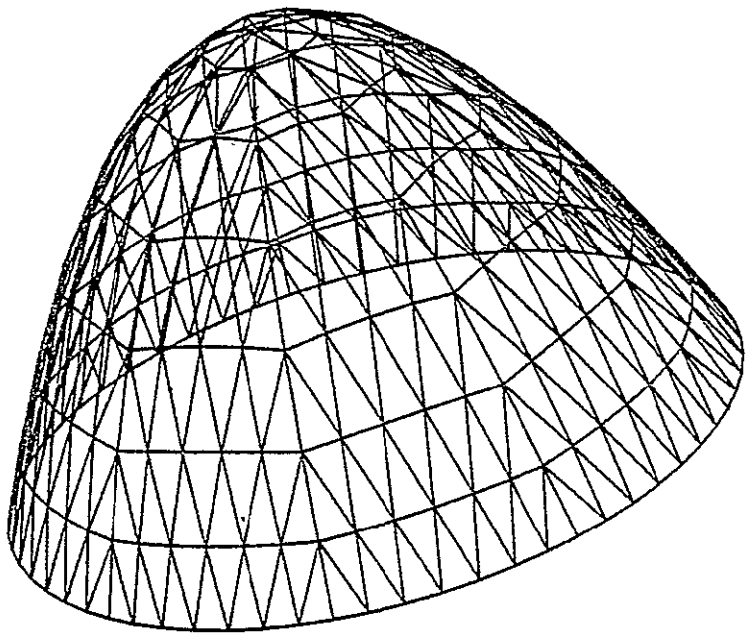

FINAL PARABOLOIDAL SHAPE

FIG. 6. PROCEDURE ILLUSTRATION OF SUBDIVISION AND BLOWING (n=8, N=7, FOD = 0.25)

known as the frequencies of the structure. The higher the frequency is, the closer one gets to the required surface. Upon further subdivisions one soon realizes, however, that the geometric constaints become enormous. Such complexity of these constaints will be discussed later on in the analysis.

III. 1 Pyramid Face Breakdown

As we mentioned earlier the pyramid represents a rather rough approximation of the required surface and that better approximations can be obtained by subdividing the individual face triangles into smaller ones and blowing them up so that their vertices will lie on the circumscribing surface.

There are many types of breakdown for the original face triangle. We here mention two of them. The first is called the "alternate breakdown" in which one draws lines parallel to the sides of the triangle. The second breakdown is known as the "triacon" and it is obtained by drawing lines perpendicular to the triangle's sides. Both breakdowns are illustrated in figure 7 for frequency 2.

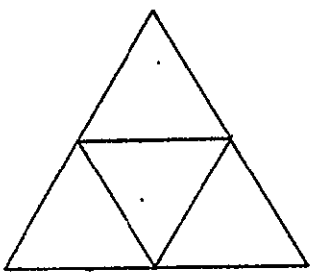

ALTERNATE

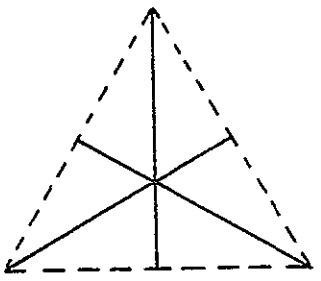

TRIACON

FIG. 7. TRIANGULAR BREAKDOWN (N=2)

There are many differences between these two kinds of breakdowns; the most obvious two are: in the alternate breakdown the original triangle edges remain part of the structure where, as in the triacon they do not and the second is that the alternate breakdown is possible in all frequencies whereas only even frequencies are possible in the case of the triacon breakdown.

In the remaining of this report we shall concentrate on describing the alternate breakdown; the triacon breakdown will be discussed in a later report. Before we further discuss the form of subdivisions we shall first adopt the following appropriate coordinate system.

The n-sided pyramid is oriented in the three dimensional rectangular coordinate system as shown in figure 8. The origin of this system is chosen to be the center of the sphere that circumscribes the pyramid, namely the sphere that passes through the points 1-n. In terms of H and R_1, the radius R of this unique sphere is given by

$$R = (R_1^2 + H^2)/2H \quad . \tag{3}$$

Accordingly, we choose the Z axis to pass through the vertex 1 with the X-Y coordinates being parallel to the aperture circle. Due to the symmetry of the pyramid faces we shall only treat a single one, namely the triangle 1,2,3 of figure 8. The projection of this triangle (1,2,3) on the horizontal plane circle is given by 1,2,3 and is shown together with the X-Y coordinate system in figure 9. With this choice of coordinate system the coordinates of the points 1,2,3 are given by

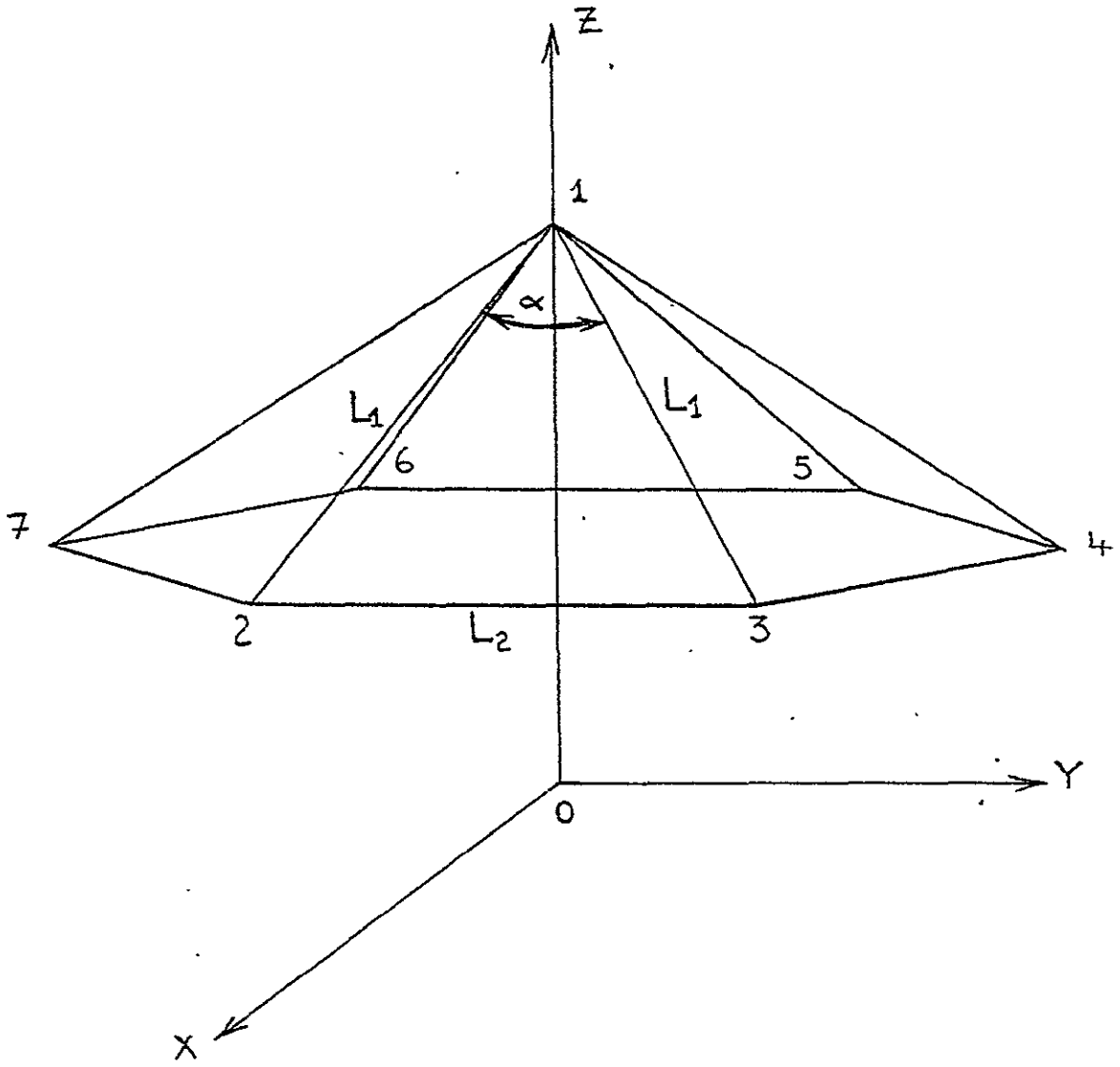

FIG. 8. APPROPRIATE COORDINATE SYSTEM

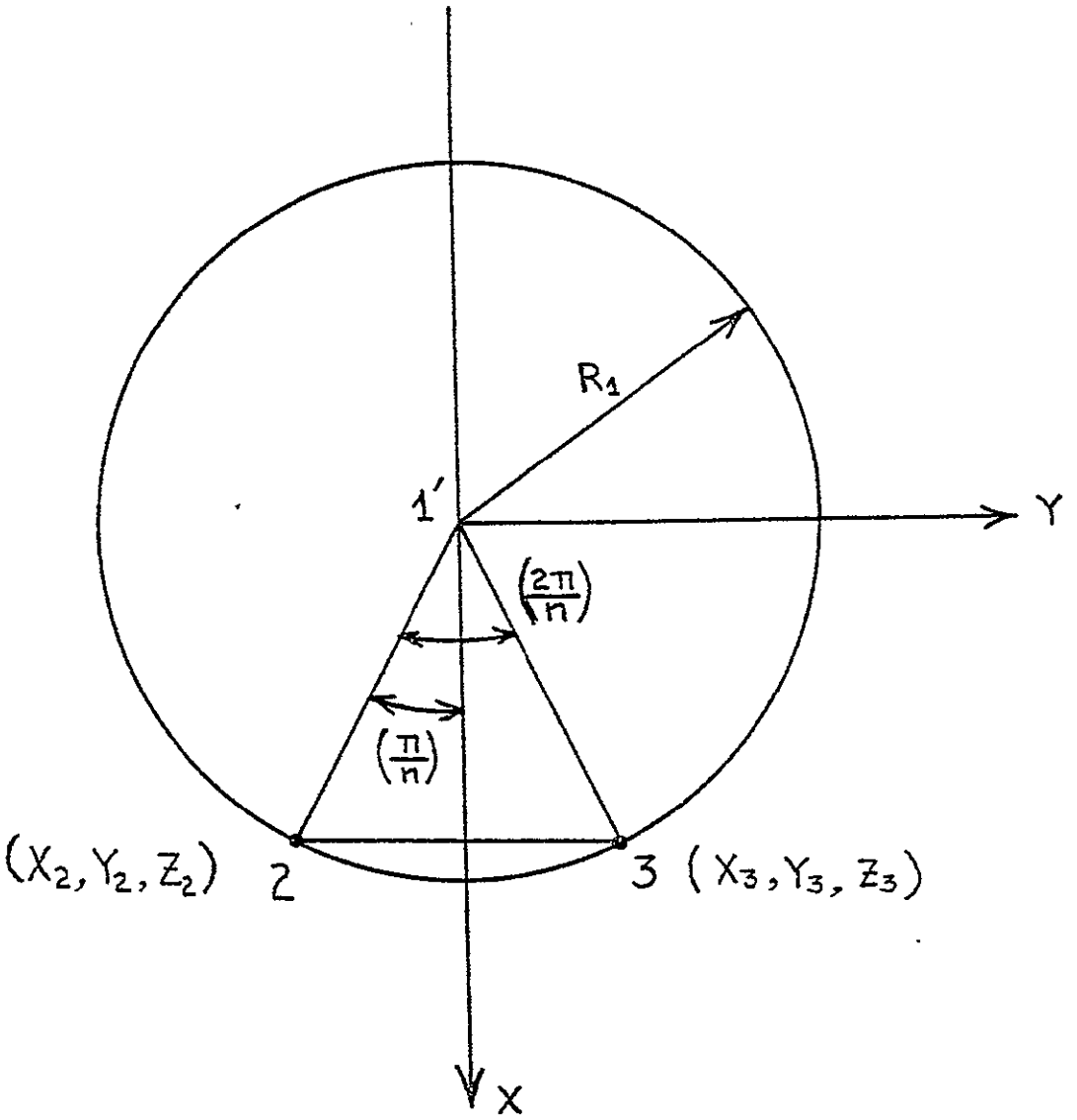

FIG. 9. PROJECTION OF TRIANGLE 1,2,3 of FIG. 8 ON THE HORIZONTAL PLANE

$$(X_1,Y_1,Z_1) = (0,0,R)$$

$$(X_2,Y_2,Z_2) = (R_1 \cos(\tfrac{\pi}{n}), -R_1 \sin(\tfrac{\pi}{n}), R-H)$$

$$(X_3,Y_3,Z_3) = (R_1 \cos(\tfrac{\pi}{n}), R_1 \sin(\tfrac{\pi}{n}), R-H) \qquad (4)$$

Notice that the coordinates of the point 1' are (0,0,R-H).

Accordingly, by subdividing the triangle 1,2,3 into frequency N as shown below in figure 10 we can determine the coordinates of the subtriangle vertices X_{JJ}, Y_{IJ}, Z_{IJ} by the alternate subdivision rule (this rule has also been employed by CIinton [10] and others).

$$X_{IJ} = X_1 + I\frac{(X_2-X_1)}{N} + J\frac{(X_3-X_2)}{N} \quad ,$$

$$Y_{JJ} = Y_1 + I\frac{(Y-Y_1)}{N} + J\frac{(Y_3-Y_2)}{N} \quad ,$$

$$Z_{IJ} = Z_1 + I\frac{(Z_2-Z_1)}{N} + J\frac{(Z_3-Z_2)}{N} \quad , \qquad (5)$$

where I and J are integers such that

$$0 \leq I \leq I \leq N$$

Notice from figure 10 that the distance between each two neighboring vertices along the 1,2 and 1,3 sides is constant and is equal to $\frac{L_1}{N}$ and that the distance between each two neighboring vertices along the 2-3 side is a constant equal to $\frac{L_2}{N}$. Now, since the coordinates of each vertex are known, its distance D_{IJ} from the origin (0,0,0), for example, is given by

$$D_{IJ} = (X_{IJ}^2 + Y_{IJ}^2 + Z_{IJ}^2)^{1/2} \qquad (6)$$

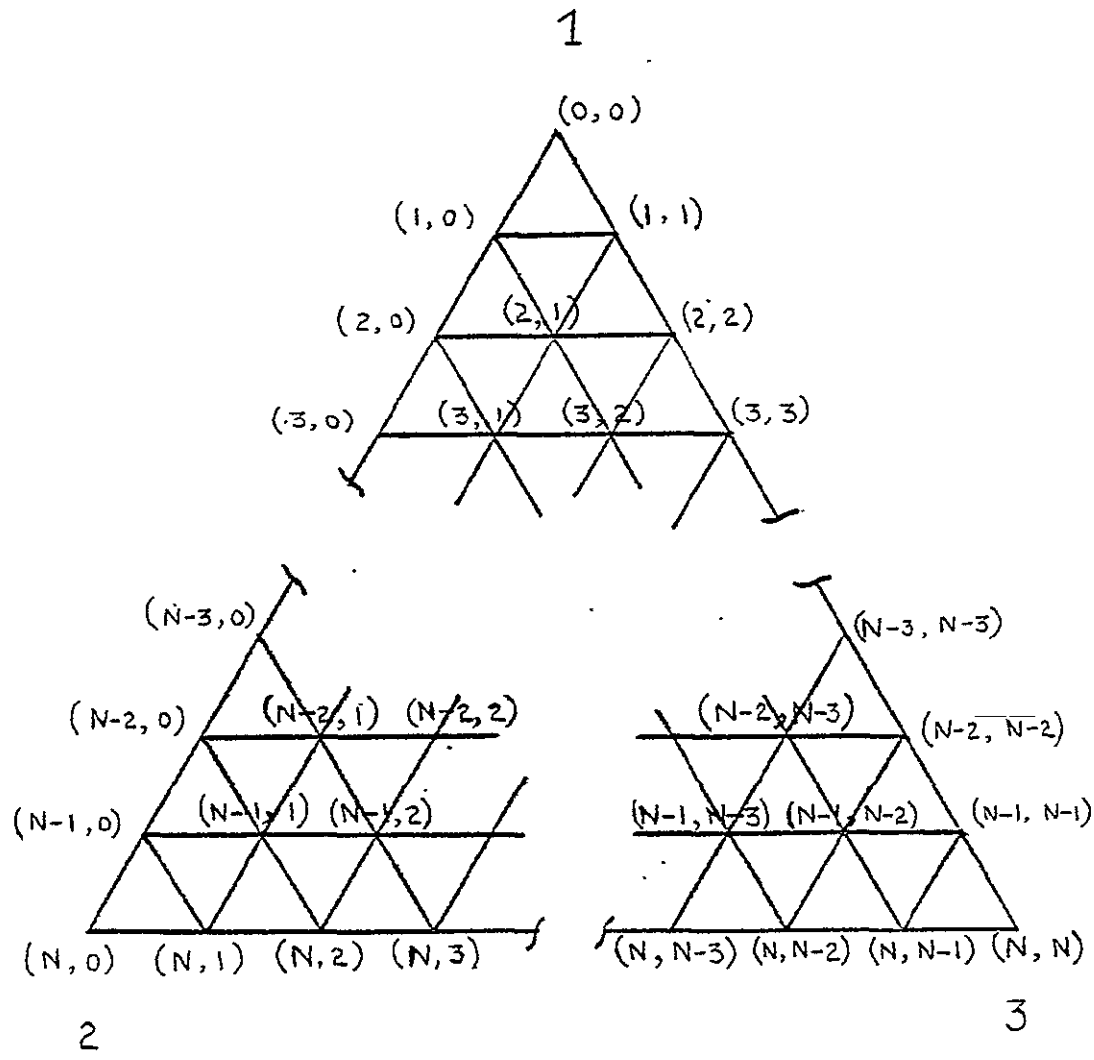

FIG.10. BREAKDOWN NUMBERING

III.2 Projections on Spherical and Paraboloidal Surfaces

In what follows we shall concentrate our efforts on developing discrete surfaces of spherical and paraboloidal cap surfaces. Simple geometric consideration will reveal that the equation of the sphere that passes through the vertices 1-n of the pyramid is given by

$$X^2 + Y^2 + Z^2 = R^2 \tag{7}$$

As for the paraboloid that passes through the points 1-n, the appropriate equation is

$$X^2 + Y^2 = \frac{R_1^2}{H}(R-Z) \tag{8}$$

(see sketch of figure 11 as an illustration of the paraboloid surface). A schematic comparison of both the spherical and paraboloidal surfaces is shown in figure 12.

III.3 Projection Centers

If the projection of the point (X_{IJ}, Y_{IJ}, Z_{IJ}) on the required surface is designated as $(X^s_{IJ}, Y^s_{IJ}, Z^s_{IJ})$, then the location of the points on the surface will depend upon their origin of projection. In what follows we shall leave the location of such a center arbitrary, namely (X_P, Y_P, Z_P).

The points $(X^s_{IJ}, Y^s_{IJ}, Z^s_{IJ})$ can be obtained by connecting the points (X_P, Y_P, Z_P) and (X_{IJ}, Y_{IJ}, Z_{IJ}) by a straight line and extending it to intersect the required solid surface. Accordingly, the equation of this straight line is

$$\frac{X^s_{IJ}-X_P}{X_{IJ}-X_P} = \frac{Y^s_{IJ}-Y_P}{Y_{IJ}-Y_P} = \frac{Z^s_{IJ}-Z_P}{Z_{IJ}-Z_P} = \begin{cases} \lambda_s & \text{for a sphere} \\ \lambda_p & \text{for a paraboloid} \end{cases} . \tag{9}$$

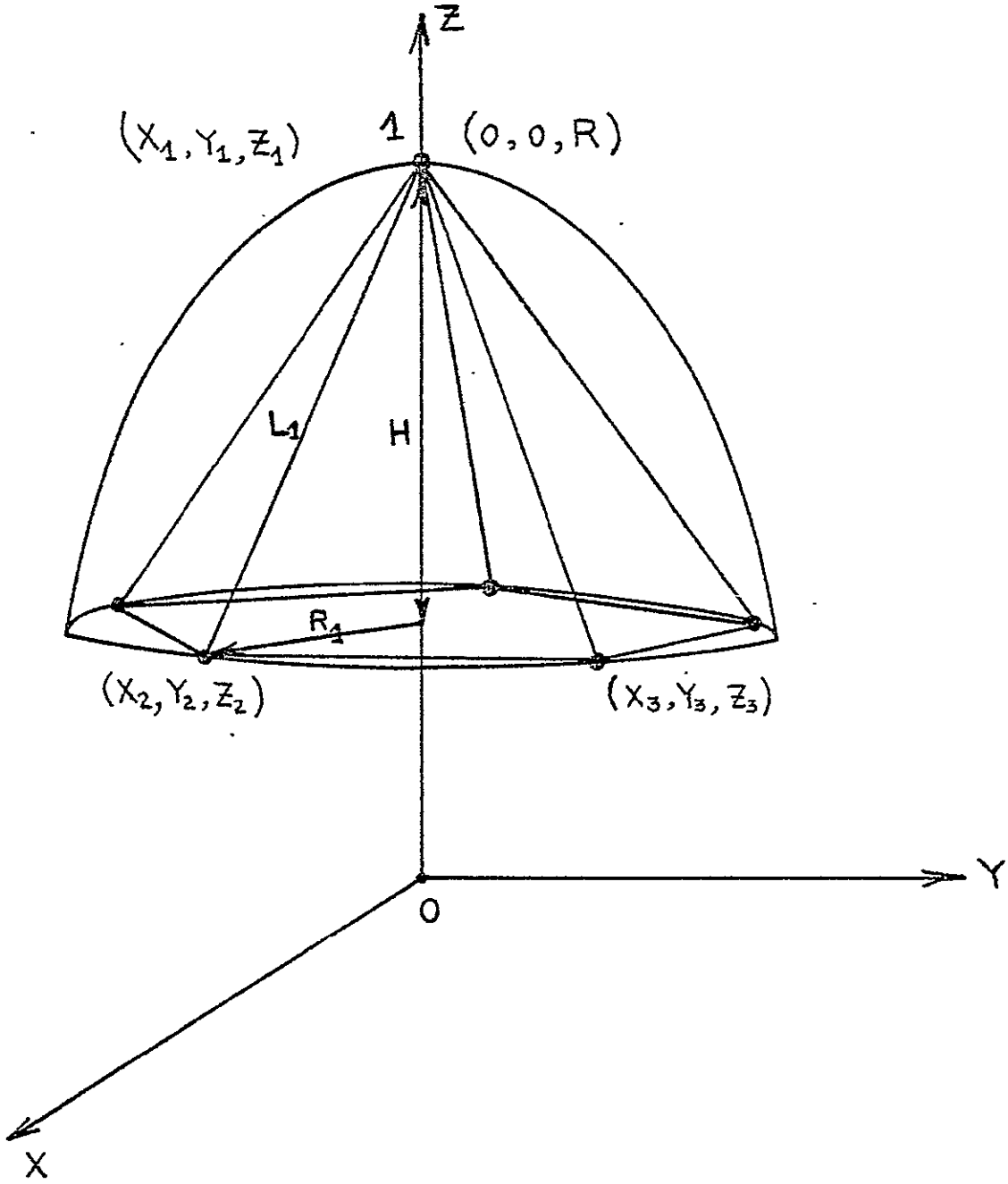

FIG. 11. EXAMPLE OF THE PARABOLOIDAL SURFACE THAT CIRCUMSCRIBES THE PYRAMID

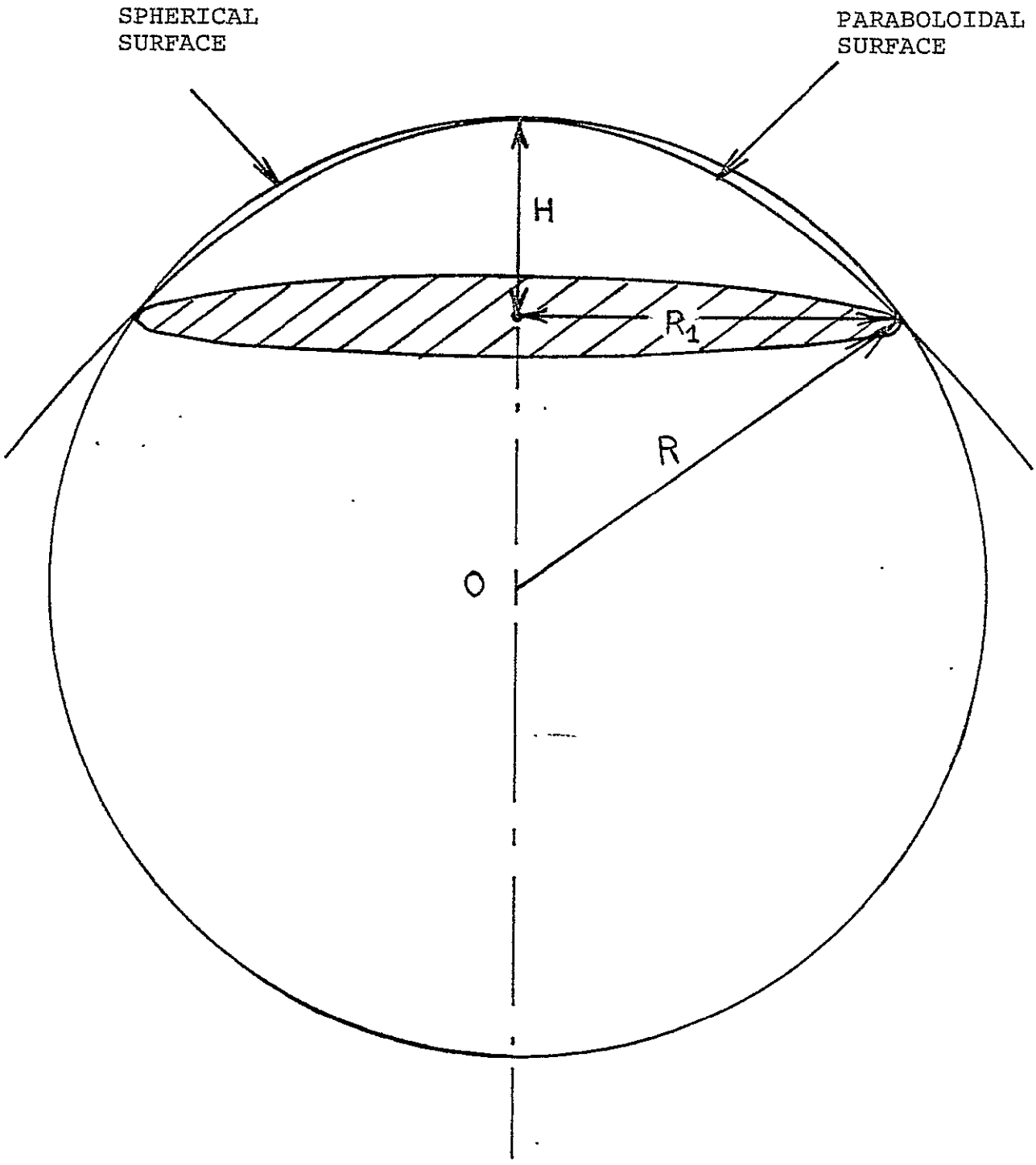

FIG. 12. COMPARISON OF PARABOLIDAL AND SPHERICAL SURFACES

Once the specific surface (sphere or paraboloid) is specified equation (9) can be solved for X^s_{IJ}, Y^s_{IJ}, Z^s_{IJ} individually in terms of the remaining quantities. For example, we obtain

$$X^s_{IJ} = \lambda_P(X_{IJ}-X_P) + X_P \tag{10}$$

for a paraboloidal surface. Similar expressions for Y^s_{IJ} and Z^s_{IJ} can be as easily obtained. Finally, substituting the resulting X^s_{IJ}, Y^s_{IJ} and Z^s_{IJ} into the appropriate equation of required solid (equation (7) for the sphere and (8) for the paraboloid) one obtains the following equations for λ_s and λ_p, respectively.

$$\lambda_s^2\left[(X_{IJ}-X_P)^2 + (Y_{IJ}-Y_P)^2 + (Z_{IJ}-Z_P)^2\right]$$

$$+ \lambda_s\left[2X_P(X_{IJ}-X_P) + 2Y_P(Y_{IJ}-Y_P) + 2Z_P(Z_{IJ}-Z_P)\right]$$

$$+\left[X_P^2 + Y_P^2 + Z_P^2 - R^2\right] = 0 \tag{11}$$

$$\lambda_P^2\left[(X_{IJ}-X_P)^2 + (Y_{IJ}-Y_P)^2\right]$$

$$+ \lambda_P\left[2X_P(X_{IJ}-X_P) + 2Y_P(Y_{IJ}-Y_P) + \frac{R_1^2}{H}(Z_{IJ}-Z_P)\right]$$

$$+\left[X_P^2 + Y_P^2 - \frac{R_1^2}{H}(R-Z_P)\right] = 0 \tag{12}$$

Each of equations (11) and (12) admits two solution. Recognizing that the cap is totally located above the location Z=0 we choose that λ which gives $Z^s_{IJ} > 0$.

III. 4 Geometric Description of Frequency N Caps

We are now in a stage where we can qualitatively describe the geometric make-up of a cap of any alternate frequency N. Here every pyramid face triangle has the number of subdivision faces s_f given by (see, for example figure 13 with N=6 for illustration)

$$s_f = \sum_{m=0}^{N-1} (2m+1) = N^2 \tag{13}$$

Hence the total number of faces in the whole cap, S_f, is

$$S_f = nN^2 \tag{14}$$

Now since from (13) each of the N^2 subtriangles has three sides and since each side is shared by two neighboring triangles, one has the total number, ℓ, of columns to build an isolated single pyramid triangle

$$\ell = \frac{3N}{2} (N+1) \tag{15}$$

Accordingly, the total number, L, of elements required for the total cap is

$$L = \frac{nN}{2} (1+3N) \tag{16}$$

Hence, an effective number of elements per each of the original pyramid triangles will be L/n. Finally, the total number, v, of vertices in the whole cap is

$$v = \left[1 + \frac{nN}{2} (N+1) \right] \tag{17}$$

III. 5 Chord Factors

Having derived expressions for the total number of members required to build the cap we now indicate that not all of these members are either equal or different in lengths. Knowing the minimum number, m, of different lengths (also known as the chord factors) is of most importance. Accordingly we now proceed to develop formulas for such a number. Generally speaking, once on

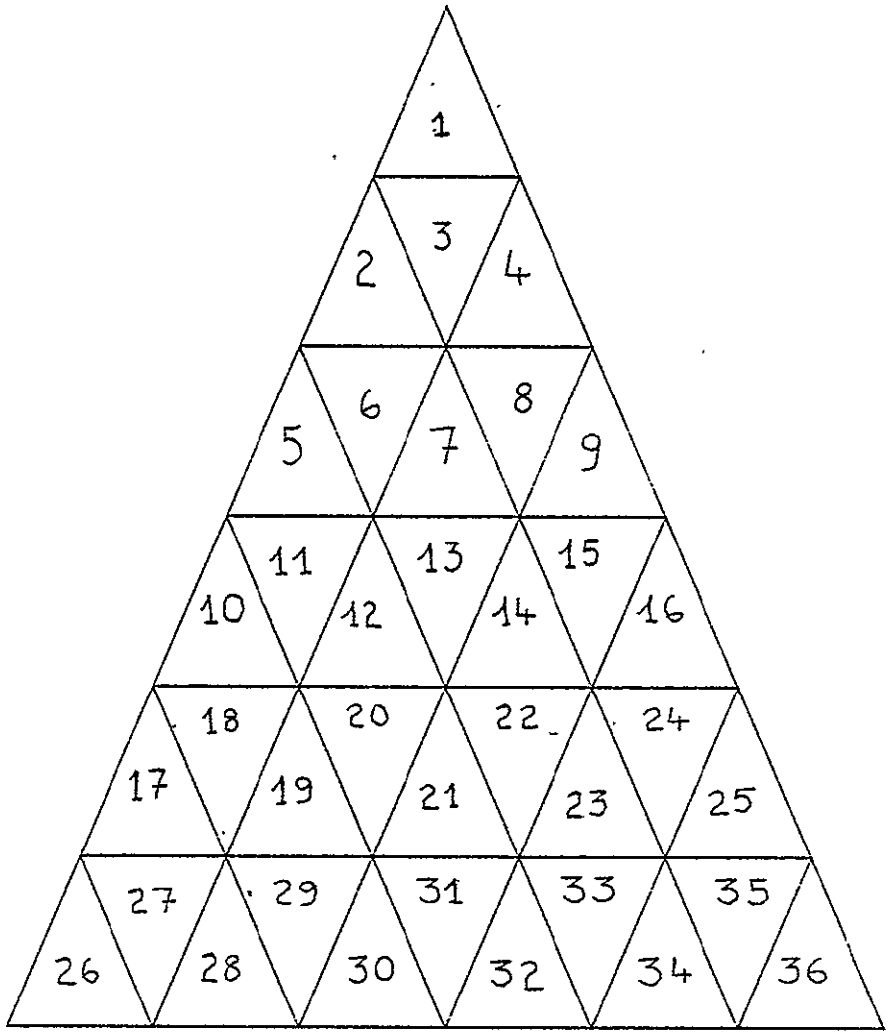

FIG. 13. NUMBER OF TRIANGULAR SUBDIVISIONS OF A PYRAMID FACE (N=6, $s_f = 36$)

the required surface the distances between neighboring vertices will not retain their original lengths. This is because of the "stretching" required to project them on the surface. In fact, these lengths will be dependent upon their original locations on the pyramid face triangle. Various symmetry relations will lead to deriving exact relations for the number of chord factors, m, required to build a given antenna. These relations are functions of the frequency N and the projection center (X_p, Y_p, Z_p) but interestingly are independent, except for a spherical surface with n=5 (see formulas below), of n (the number of the sides of the original pyramid). These relations are listed as:

(a) For a paraboloidal surface with projection center $(0,0,Z_p)$ where Z_p is an arbitrary variable

$$m = \frac{3}{4} N^2 + N + \frac{1}{4} \text{ , (N odd, see Fig. 14 for illustrative symmetry)} \quad (18)$$

$$m = \frac{3}{4} N^2 + N \text{ , (N even, see Fig. 15 for illustrative symmetry)} \quad (19)$$

(b) For a spherical surface we have the following formulas depending upon the projection center and n

(i) center of projection (0,0,0) and $n \neq 5$

$$m = \frac{3}{4} N^2 + \frac{N}{2} + \frac{3}{4} \text{ , (N odd, see Fig. 16 for illustrative symmetry)} \quad (20)$$

$$m = \frac{3}{4} N^2 + \frac{N}{2} \text{ , (N even, see Fig. 17 for illustrative symmetry)} \quad (21)$$

(ii) center of projection (0,0,0), n=5 and $L_1 = L_2$ (Fuller's case)

$$m = \frac{1}{4} [(N+1)^2 - 1] \text{ , (N even and not multiple of 3), (see Fig. 18 for illustrative symmetry)} \quad (22)$$

$m = \frac{1}{4}(N+1)^2$, (N odd and not multiple of 3), (see Fig. 19 for illustrative symmetry) (23)

$m = \frac{N}{2}(\frac{N}{3} + 1)$, (N multiple of 3), (see Fig. 20 for illustrative symmetry) (24)

(iii) center of projection $(0,0,Z_P)$, with $Z_P \neq 0$

$m = \frac{3}{4}N^2 + N + \frac{1}{4}$, (N odd, see Fig. 14 for illustrative symmetry) (25)

$m = \frac{3}{4}N^2 + N$, (N even, see Fig. 15 for illustrative symmetry) (26)

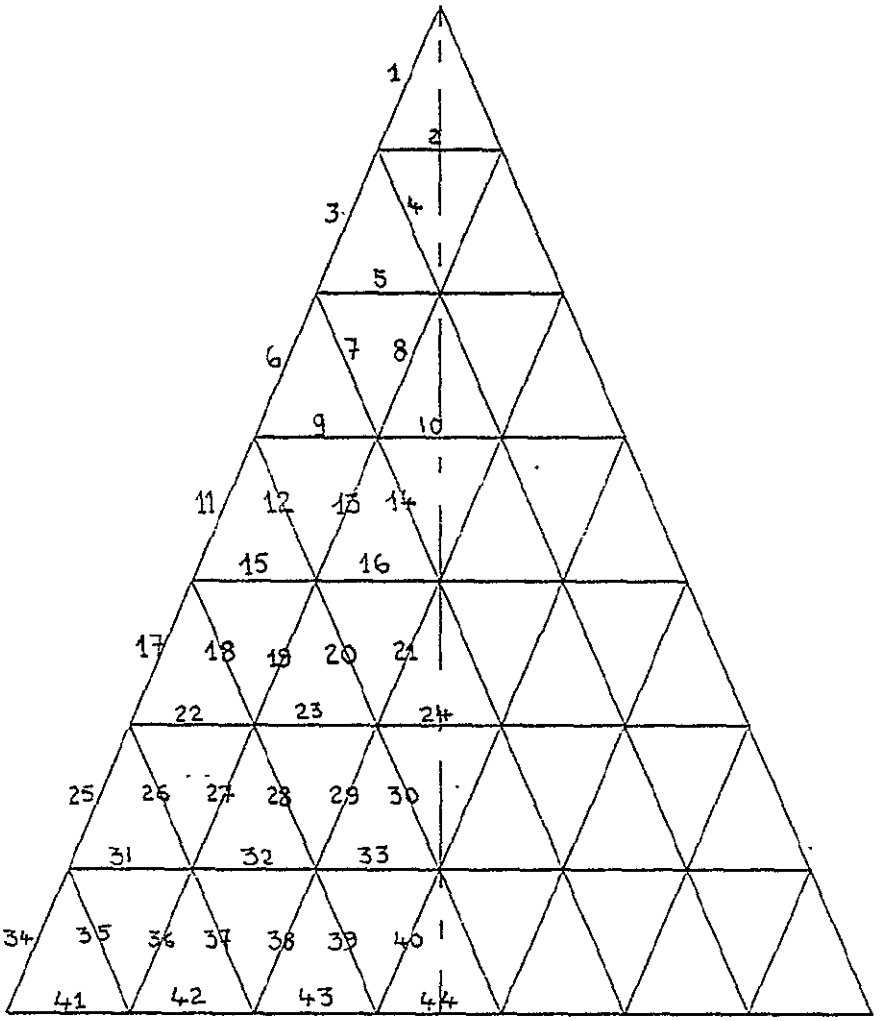

FIG. 14. NUMBER OF CHORD FACTORS AS PREDICTED BY EQUATION (18)

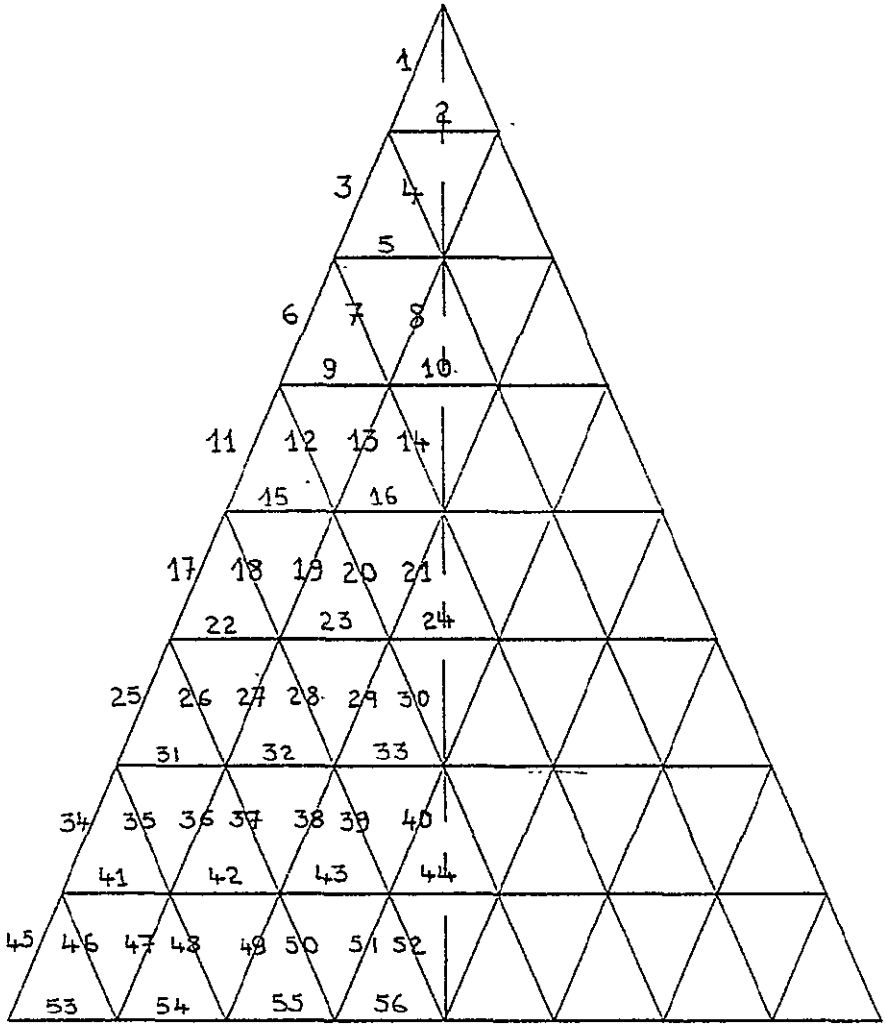

FIG. 15. NUMBER OF CHORD FACTORS AS PREDICTED BY EQUATION (19)

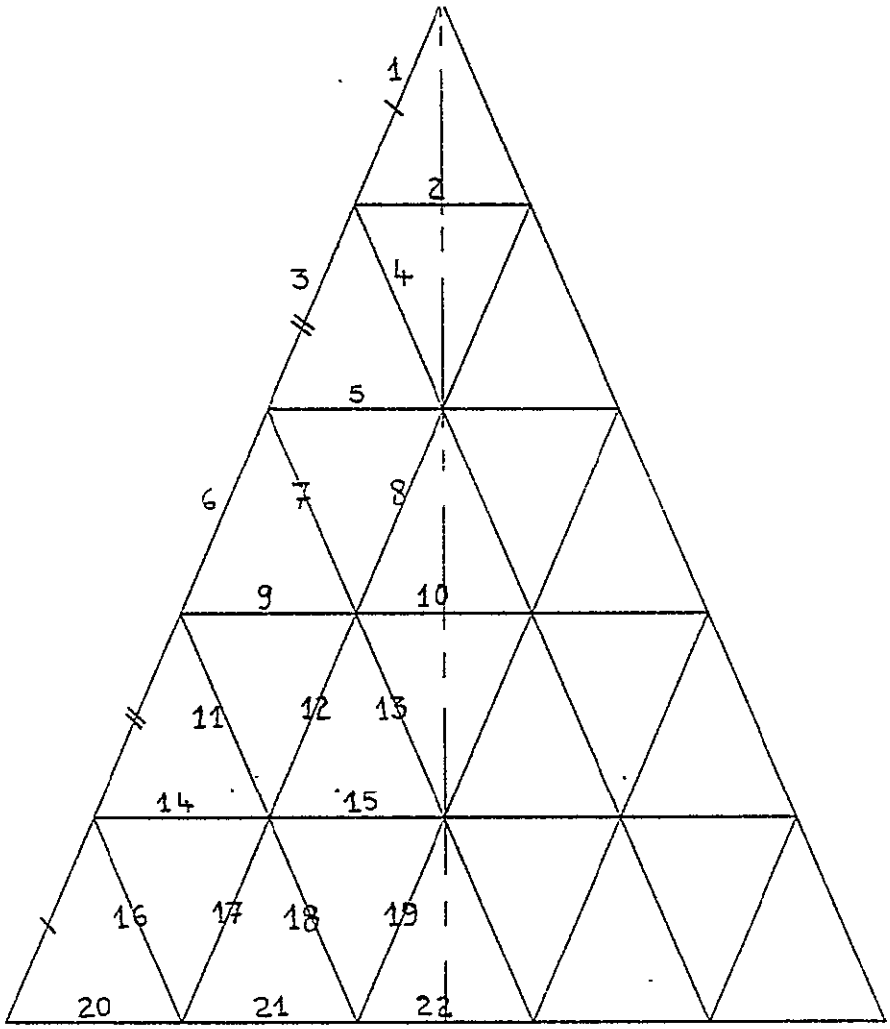

FIG. 16. NUMBER OF CHORD FACTORS AS PREDICTED BY EQUATION (20)

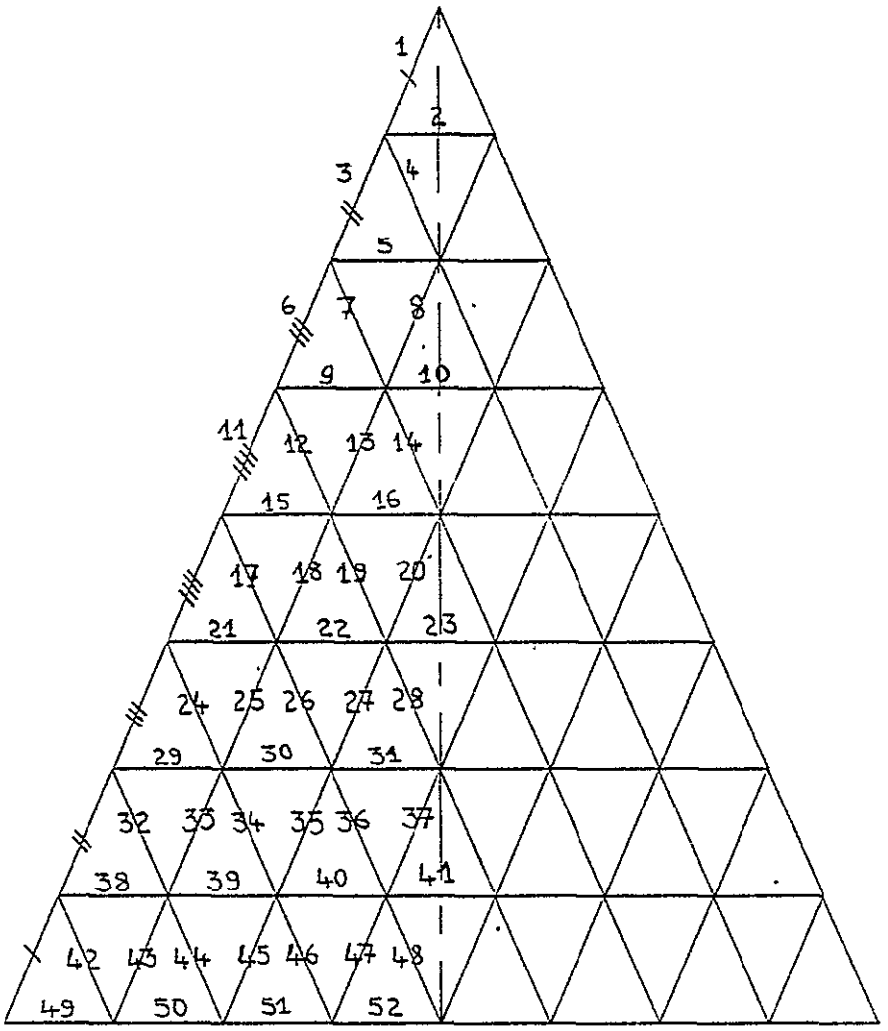

FIG. 17. NUMBER OF CHORD FACTORS AS PREDICTED BY EQUATION (21)

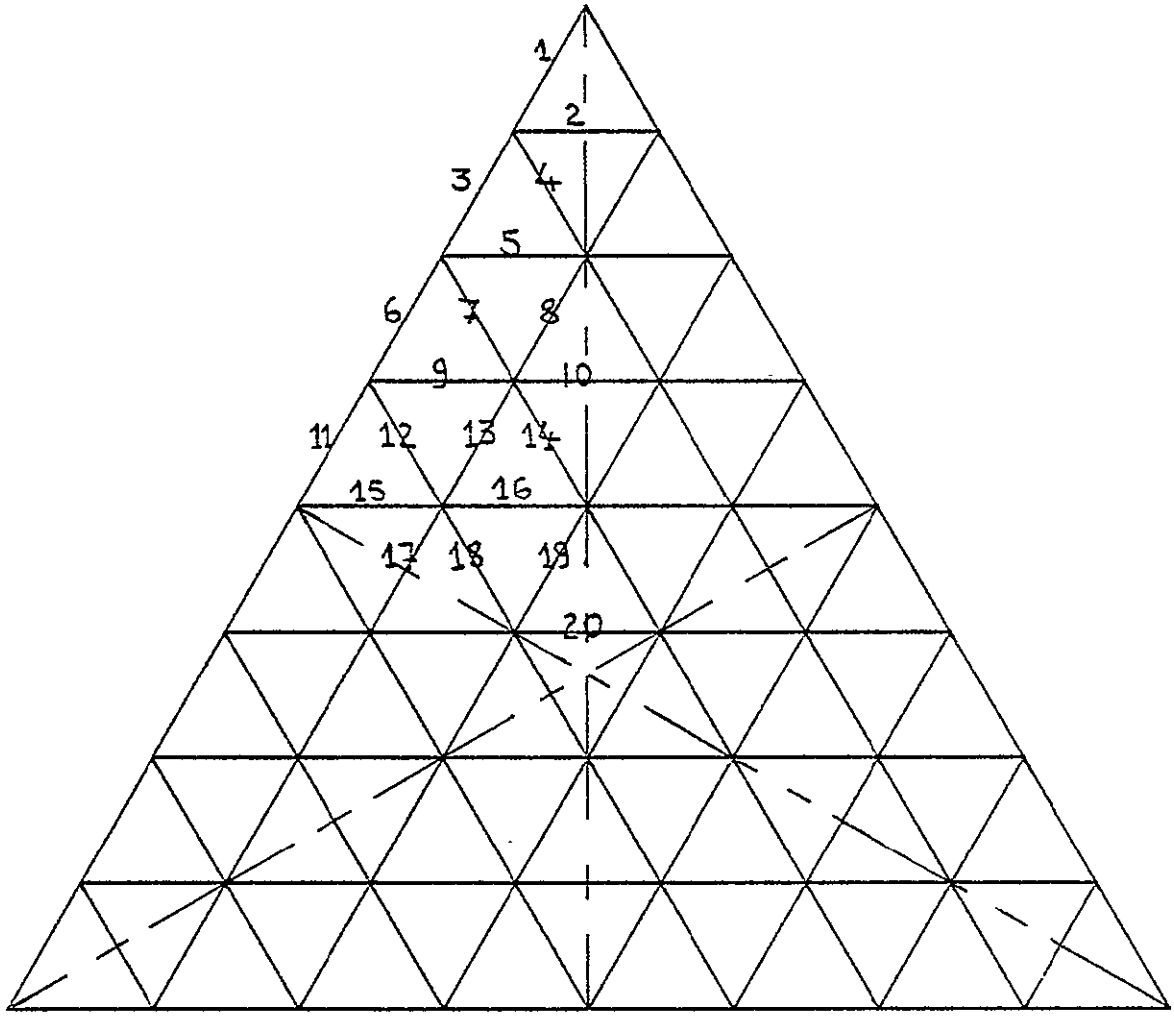

FIG. 18. NUMBER OF CHORD FACTORS AS PREDICTED BY EQUATION (22)

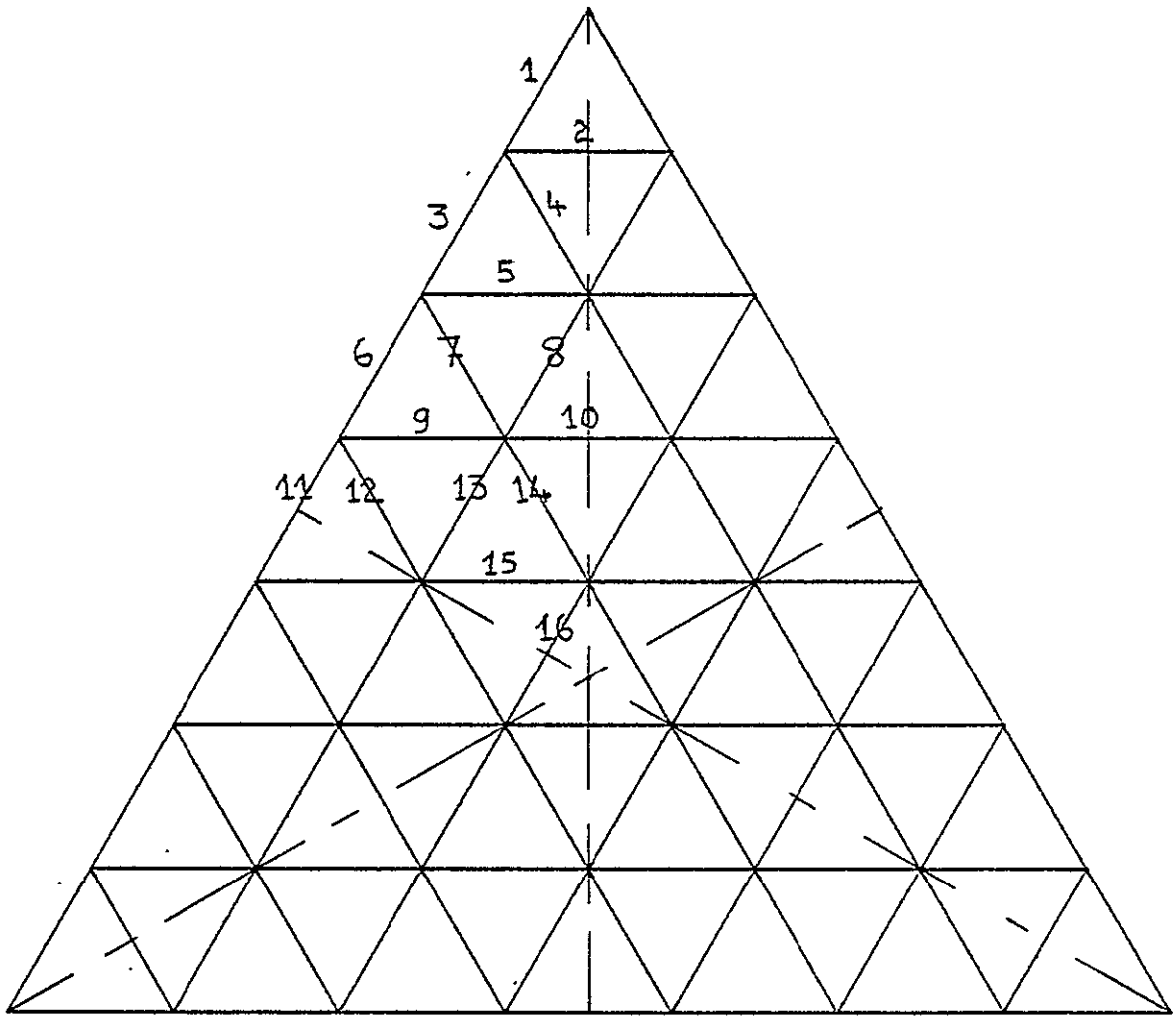

FIG. 19. NUMBER OF CHORD FACTORS AS PREDICTED BY EQUATION (23)

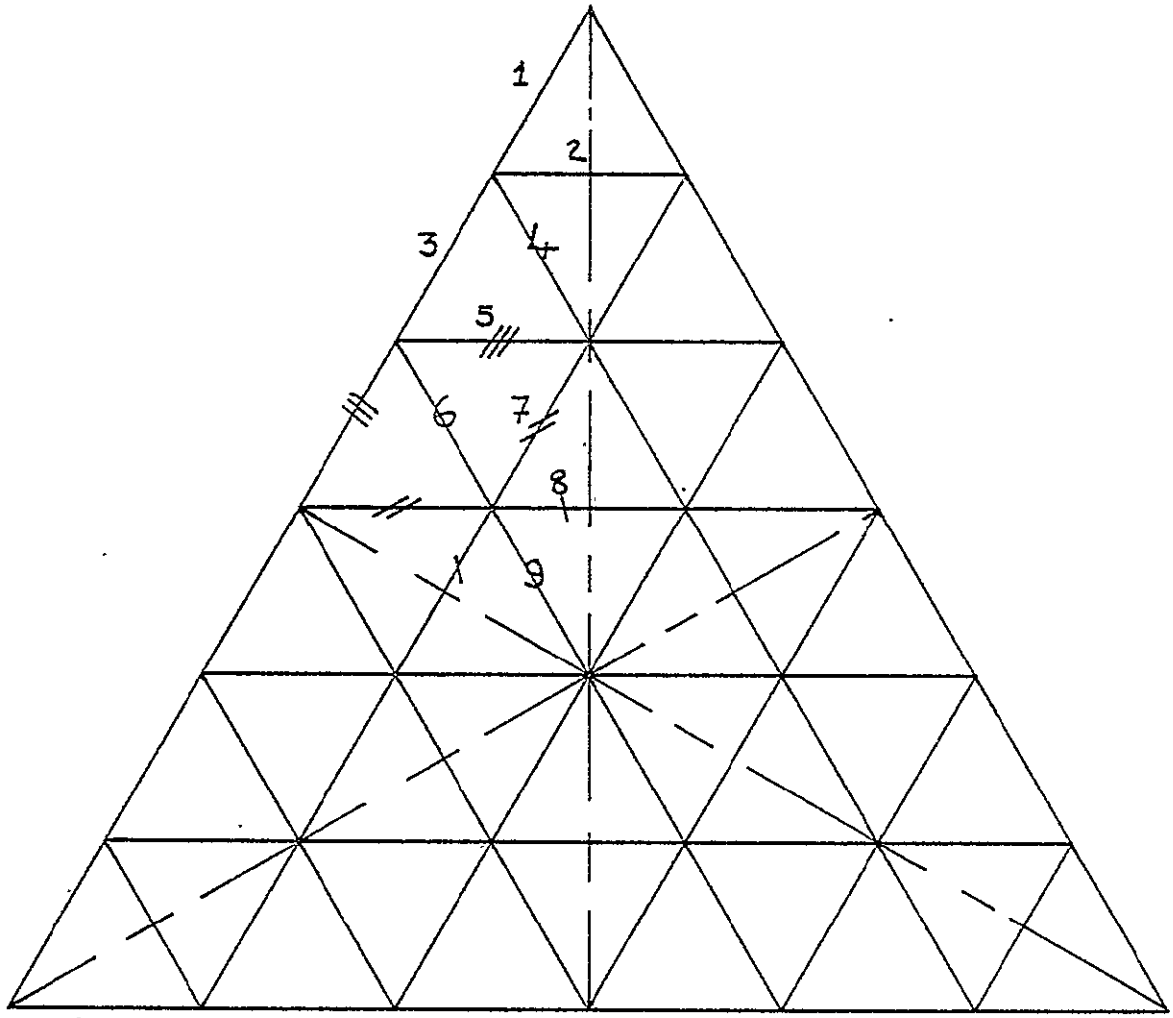

FIG. 20. NUMBER OF CHORD FACTORS AS PREDICTED BY EQUATION (24)

III. 6 Normal Projections from the Intersections of 0, $\pm 60^{o}$ Array

An interesting special case of our modeling subdivision and blowing can be obtained by choosing the vertex1' whose coordinates are (0,0,R-H) rather than the vertex 1 whose coordinates are (0,0,R) for our reference "pyramid". If subsequently we project, for any frequency N, from the center $(0,0,Z_p)$ with $Z_p \to \infty$ we obtain the results for the case where normal projections are carried out from each of the intersection of 0, $\pm 60^{o}$ flat array to meet the surface of the solid (see figure 21 for complete procedure illustration).

Exact results for this special case can also be obtained as follows: by setting $X_1 = 0$, $Y_1 = 0$ and $Z_1 = R-H$ in equation (4) we adapt it to the 0, $\pm 60^{o}$ flat array subdivision of the aperture circle. For every point (X_{IJ}, Y_{IJ}, Z_{IJ}) we raise a normal to the flat array which meets the required surface at the point $(X^s_{IJ}, Y^s_{IJ}, Z^s_{IJ})$ which is uniquely determined once the surface is specified as follows: For the sphere one has

$$(X^s_{IJ}, Y^s_{IJ}, Z^s_{IJ}) = (X_{IJ}, Y_{IJ}, \sqrt{R^2-(X^2_{IJ}+Y^2_{IJ})}) \tag{23}$$

and for the paraboloid one has

$$(X^s_{IJ}, Y^s_{IJ}, Z^s_{IJ}) = (X_{IJ}, Y_{IJ}, [R - \frac{H}{R_1^2}(X^2_{IJ}+Y^2_{IJ})]) \tag{24}$$

Once the points on the surface are specified the calculations follows exactly the steps of the alternate breakdown outlined above.

As will be shown numerically later on both the results of the exact procedure of equations (23) and (24) will be indistinguishable, as far as member lengths and smoothness are concerned from the limiting case of the alternate breakdown with the projection center $(0,0,Z_p)$ with $Z_p \to \infty$. It will also be shown that the number of chord factors will dramatically decrease for the "normal projection"

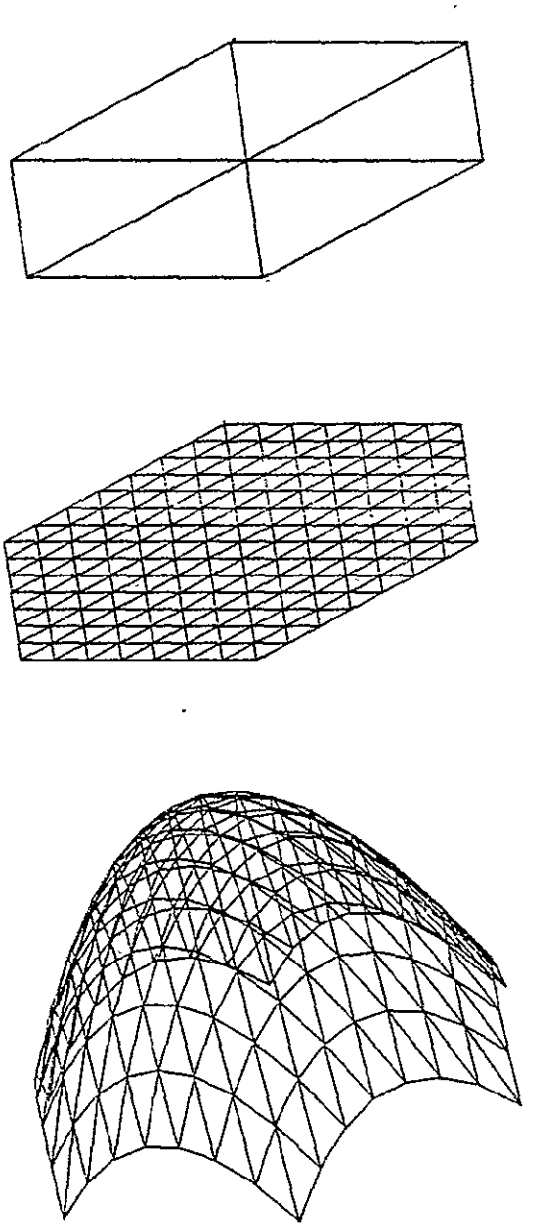

FIG. 21. PROCEDURE ILLUSTRATION OF SUBDIVISION AND NORMAL PROJECTION BLOWING (n=6, N=7, FOD = 0.25)

modeling especially for the case of the paraboloid surface.

III.7 Measure of Smoothness

As we mentioned earlier the higher the frequency N is, the better the discrete system will approximate the required solid surface. An important measure of such approximation (smoothness) is the magnitude of the maximum distance between the subdivision triangles and solid surface. We refer to this measure as δ. It is obvious that for a given cap geometry the value of δ will decrease with increasing frequency. It is also obvious that δ will decrease with increasing n. In order to determine δ, we proceed as follows.

Generally speaking the equation of a flat plane P passing through the three arbitrary points (X_1,Y_1,Z_1), (X_2,Y_2,Z_2) and (X_3,Y_3,Z_3) is given by

$$\begin{vmatrix} X & Y & Z & 1 \\ X_1 & Y_1 & Z_1 & 1 \\ X_2 & Y_2 & Z_2 & 1 \\ X_3 & Y_3 & Z_3 & 1 \end{vmatrix} = 0 \qquad (25)$$

or equivalently by

$$AX + BY + CZ + D = 0 \qquad (26a)$$

where

$$A = \begin{vmatrix} Y_1 & Z_1 & 1 \\ Y_2 & Z_2 & 1 \\ Y_3 & Z_3 & 1 \end{vmatrix}, \quad B = -\begin{vmatrix} X_1 & Z_1 & 1 \\ X_2 & Z_2 & 1 \\ X_3 & Z_3 & 1 \end{vmatrix} \qquad (26b,c)$$

$$C = \begin{vmatrix} X_1 & Y_1 & 1 \\ X_2 & Y_2 & 1 \\ X_3 & Y_3 & 1 \end{vmatrix}, \quad D = -\begin{vmatrix} X_1 & Y_1 & Z_1 \\ X_2 & Y_2 & Z_2 \\ X_3 & Y_3 & Z_3 \end{vmatrix} \qquad (26d,e)$$

Let us suppose that another curved surface S (such as a paraboloid for example) passes through these three points. The maximum distance between the plane P and the surface S (see figure 22) is the normal distance between the plane P and the tangent plane T to S which is parallel to P; this distance is shown as N_1, N_2 in figure 22 . The directions ratio of N_1 N_2 are given by

$$A : B : C \tag{27}$$

since N_1 N_2 is perpendicular to the planes P and T. Using the above analysis, we can determine the maximum derivation for any surface, particularly those of the spherical and paraboloidal as follows

Spherical Surface:

The equation of spherical surface is given by (see equation 7),

$$X^2 + Y^2 + Z^2 = R^2 \tag{28}$$

Accordingly the direction cosines of any perpendicular to this surface are given by:

$$\frac{\partial F}{\partial X} : \frac{\partial F}{\partial Y} : \frac{\partial F}{\partial Z} \tag{29}$$

where the function F is given by

$$F = (X^2 + Y^2 + Z^2 - R^2) \tag{30}$$

At the particular point N_2 (the parallel tangent point), these direction ratios must be the same as those of (27); this implies

$$\frac{\partial F}{\partial X} : \frac{\partial F}{\partial Y} : \frac{\partial F}{\partial Z} = A : B : C \tag{31}$$

which from (30) yields

$$A : B : C \doteq X : Y : Z \tag{32}$$

Equation (32) can thus be rewritten as

$$\frac{A}{X} = \frac{B}{Y} = \frac{C}{Z} = \lambda \tag{33}$$

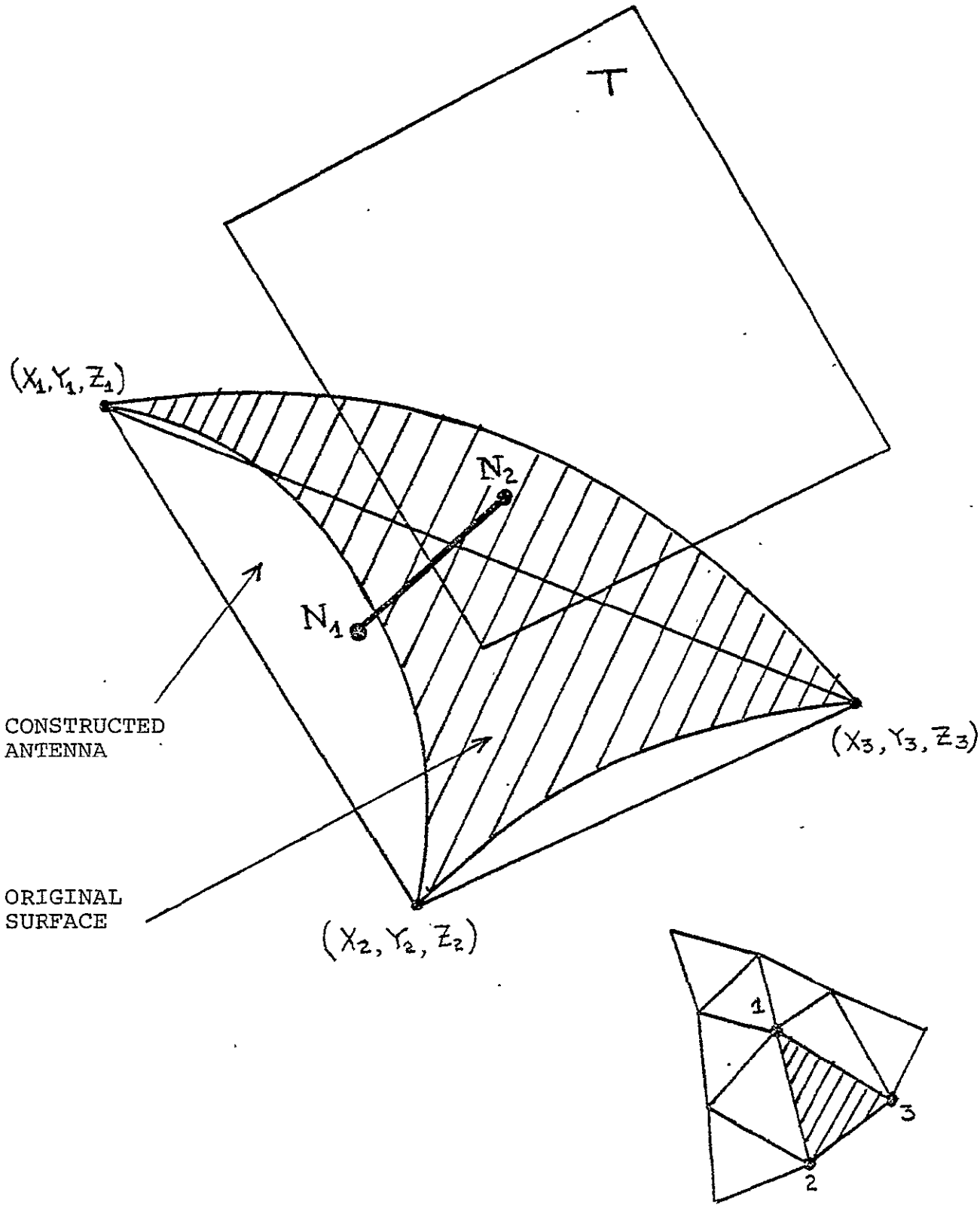

FIG. 22. DISPLAY OF ACTUAL SOLID SURFACE AND ITS TANGENT

where λ is to be determined. Substituting from (33) into (28) we determine the coordinates of the point $N_2 = (X^B, Y^B, Z^B)$ as

$$X^B = A/\lambda \ , \quad Y^B = B/\lambda \ , \quad Z^B = C/\lambda \tag{34}$$

and hence λ is given by

$$\lambda = (A^2 + B^2 + C^2)^{1/2}/R \tag{35}$$

Now, the maximum distance δ between the plane P and the surface of the sphere is given by the distance between the point N_2 and the plane P which is known as

$$\delta = \frac{AX^B+BY^B+CZ^B+D}{\sqrt{A^2 + B^2 + C^2}} \tag{36}$$

Paraboloidal Surface:

For the paraboloidal surface the function F is given by

$$F = (X^2 + Y^2 + \frac{R_1^2}{H} Z - \frac{RR_1^2}{H}) \quad . \tag{37}$$

Using the same analysis used for the sphere one gets

$$\frac{\partial F}{\partial X} \ : \ \frac{\partial F}{\partial Y} \ + \ \frac{\partial F}{\partial Z} = A \ : \ B \ : \ C \tag{38}$$

or equivalently

$$\frac{A}{2X} = \frac{B}{2Y} = \frac{C}{R_1^2/H} \ = \ \lambda \tag{39}$$

Accordingly the coordinates of the point N_2 are given by

$$X^B = A/(2\lambda) \ , \ Y^B = B/(2\lambda) \ , \ Z^B = R - \frac{H\{(X^B)^2+(Y^B)^2\}}{R_1^2} \tag{40}$$

where λ is given by

$$\lambda = HC/R_1^2 \tag{41}$$

The maximum derivation can again be calculated using the formula 36.

IV. COMPUTER CODE CALCULATIONS

A general purpose computer code has been written in order to model discrete rod-like shells of revolutions as outlined above. This code contains many possible combinations of design parameters which we have mentioned in our analysis. The code also contains a general and self sufficient graphical subroutine. To see how both the computational (modeling) and graphical codes work we have first to define their parameters and then proceed to study their flow chart. The graphical subroutine is described in Appendix A.

Input Parameters:

FϕD = focus to aperture diameter ratio.

AP≡D = aperture diameter.

NS≡n = number of equal subdivisions of aperture circle.

LT = Shell type: { 1 Sphere; 2 Paraboloid

(XP, YP, ZP) = Coordinates of the center of projection.

LN = Design control card: { 1 Single center of projection method; 2 Normal projection method

N = frequency of subdivision

AA1, AA2, AA3 = α_1, α_2, α_3 = Euler's angles

EPSL = constant used in the parametric study of chord factors.

Calculated Parameters:

R1 = AP/2 = radius of the aperture circle

H = height of the cap

(X1, Y1, Z1) , (X2, Y2, Z2) , (X3, Y3, Z3) are the coordindates of the representative triangle face (1,2,3) (see Sketch 1).

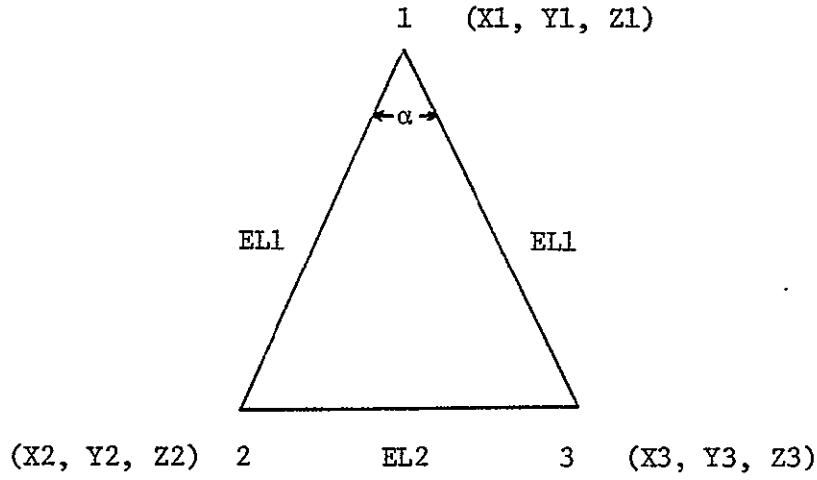

Triangular Face
SKETCH I

EL1, EL2, α properties of the triangular face.

$X^S(I,J)$, $Y^S(I,J)$, $Z^S(I,J)$ coordinates of the projected point on the surface of the cap.

D1(I,J), D2(I,J), D3(I,J) the side lengths of the subtriangles.

G(I)≡m = different chord lengths.

GG(I) = different normalized chord factors.

GGMX = length of the longest chord.

GGMN = lenth of the minimum chord.

IK≡m = numerical number of the chord factors.

NFF≡m = analytical number of the chord factors.

LMN = numerical number of the parameterized chord factors for a given EPSL.

GN(LMN) = parameterized chord factors.

XMAX≡δ = maximum deviation.

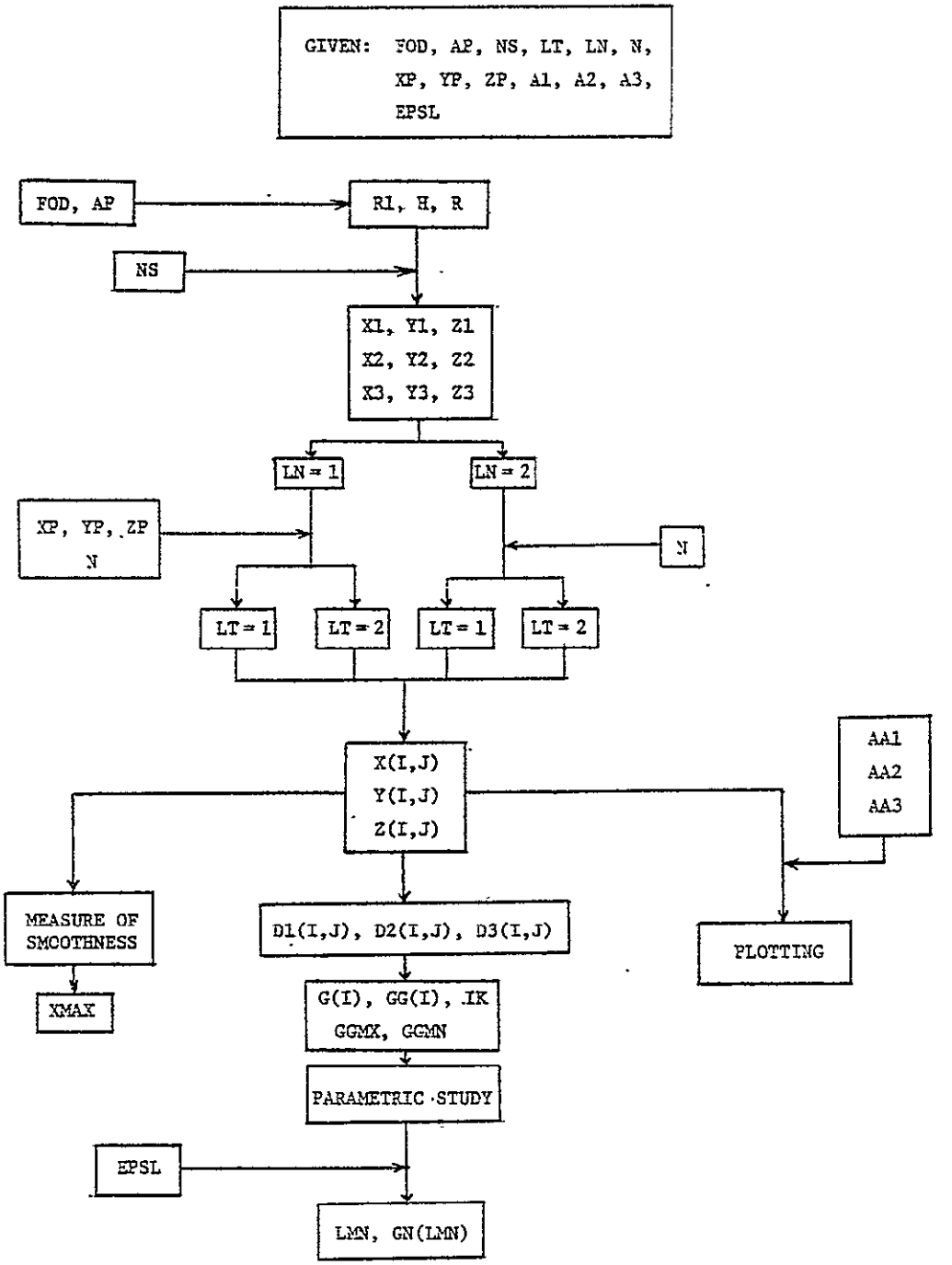

COMPUTER PROGRAM FLOW CHART

WE INTEND TO SUBMIT THE COMPUTER PROGRAM TO COSMIC. IN THE MEANWHILE THE PROGRAM WILL BE AVAILABLE FROM THE AUTHORS.

V. ILLUSTRATIVE RESULTS

The utility of our general computer program will be demonstrated by generating necessary design parameters of discrete large space antenna reflectors. Specifically we determine the shape and size of flat segmented surfaces which approximate spherical and paraboloidal reflector surfaces. Our results will also be displayed in the form of compressions between the spherical and paraboloidal designs. Results will be presented for a wide range of proportions; focus-to-diameter (F/D) radius from .25 to 1 which go all the way from a hemisphere to a very shallow dish. Other important parameters which may vary are the number of pyramid faces, n, the frequency of subdivision, N and the aperture diameter D.

We have carried our numerical calculation on an antenna with the common fixed properties D = 100m, n = 6 and N = 10 and the variable properties FOD and the center of projection. In Figure 23, a plot of L_{max} and L_{min} for both spherical and paraboloidal dishes shown as functions of FOD for two different projection centers namely the center of the sphere (0,0,0) and (0,0, -10^6R) (this second projection center is equivalent to the normal projection method of Section III.6). In Figure 24 various plots of $\frac{L_{min}}{L_{max}}$ are shown as functions of FOD for the three projection centers (0,0,R-H), (0,0,0) and (0,0, -10^6R). In Figure 25 a variation of $\frac{L_{min}}{L_{max}}$ as a function of projection center is depicted for FOD = 1 for the paraboloidal surface. As may be seen, the best projection center is that which is around (0,0, -R) where $\frac{L_{min}}{L_{max}} = .985$. The corresponding results for FOD = 0.25 and for a spherical surface is shown in Figure 26. The variation of δ as a function of frequency N is shown in Figure 30 for various FOD values for both spherical and paraboloidal surfaces.

The variation of δ with FOD is shown in Figure 29 for various projection centers. Finally a variation of $\frac{L_{min}}{L_{max}}$ as a function of n (for an FOD = 1 paraboloidal dish) is shown in Figure 28 for two different projection centers.

As may be easily seen from this figure the $\frac{L_{min}}{L_{max}}$ can be obtained for n = 6 with the projection center being (0,0,0). The variation of this max value of $(\frac{L_{min}}{L_{max}})$ with the frequency is shown in Figure 27. Varying the frequency will alter very slightly this value.

From the above figures one can easily draw the conclusion that the $\frac{L_{max}}{L_{min}}$ increases with increasing FOD where both the spherical and the paraboloidal dishes are practically indistinguishable. On the other hand for lower FOD it appears that $\frac{L_{max}}{L_{min}}$ is much higher for the paraboloid as compared with the sphere.

Finally, for the plotting illustrations we depict in figures 31 and 32 plots of a variety of dishes. On each plot we list the necessary parameters used.

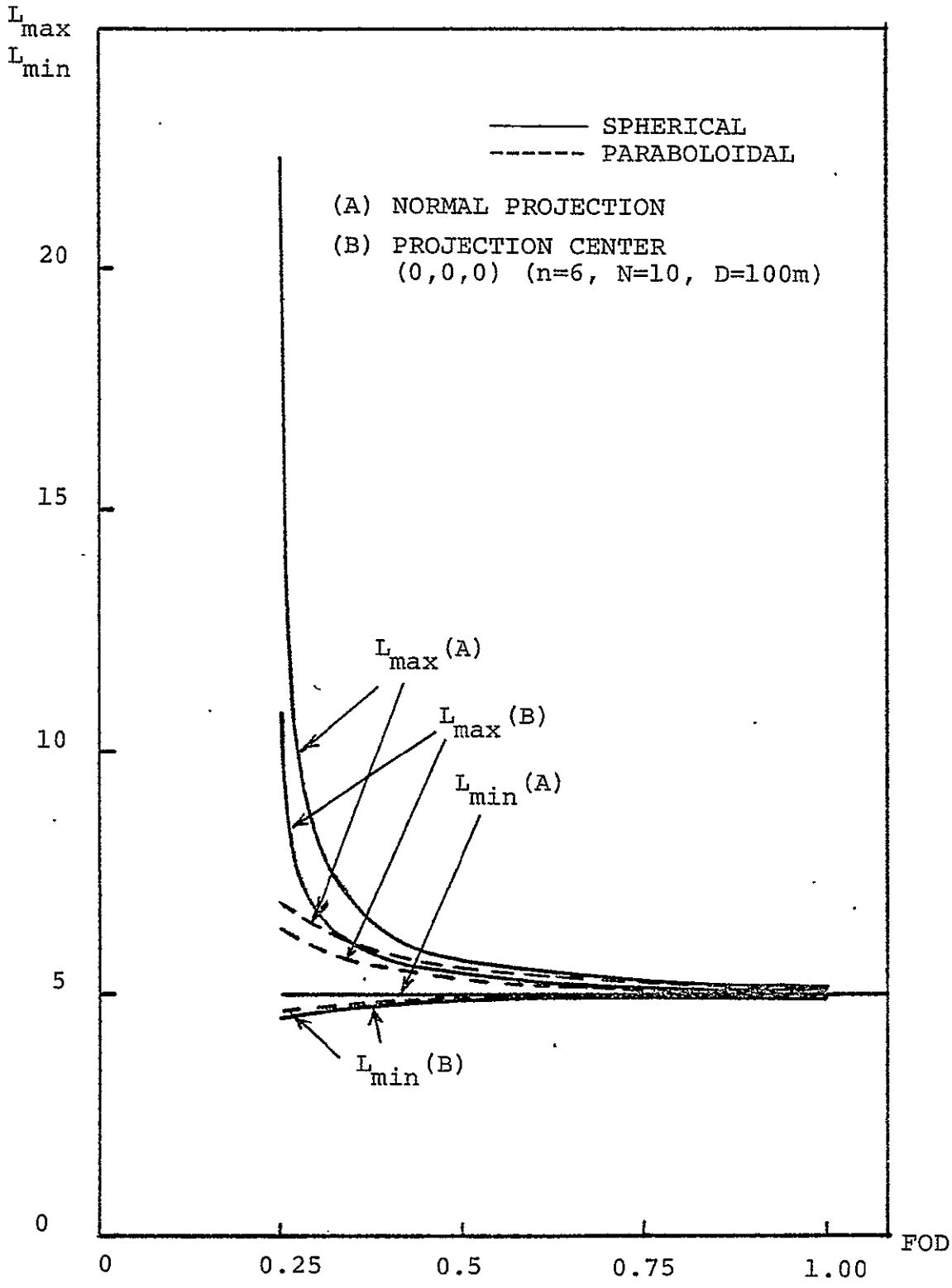

FIG. 23. VARIATION L_{max} AND L_{min} WITH FOD FOR A TWO PROJECTION CENTER

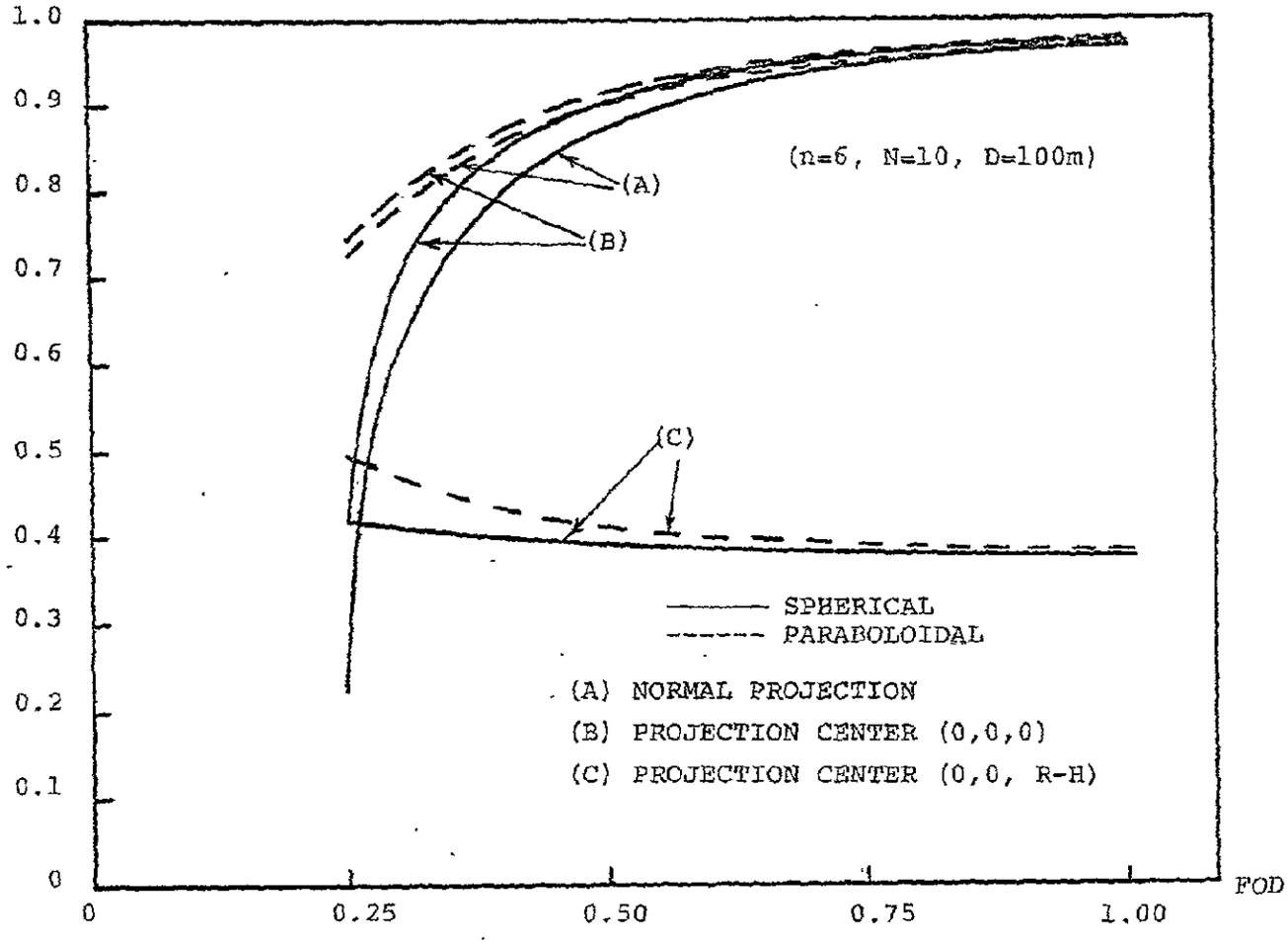

FIG. 24. VARIATION OF $\frac{L_{min}}{L_{max}}$ WITH FOD FOR A VARIETY OF PROJECTION CENTERS

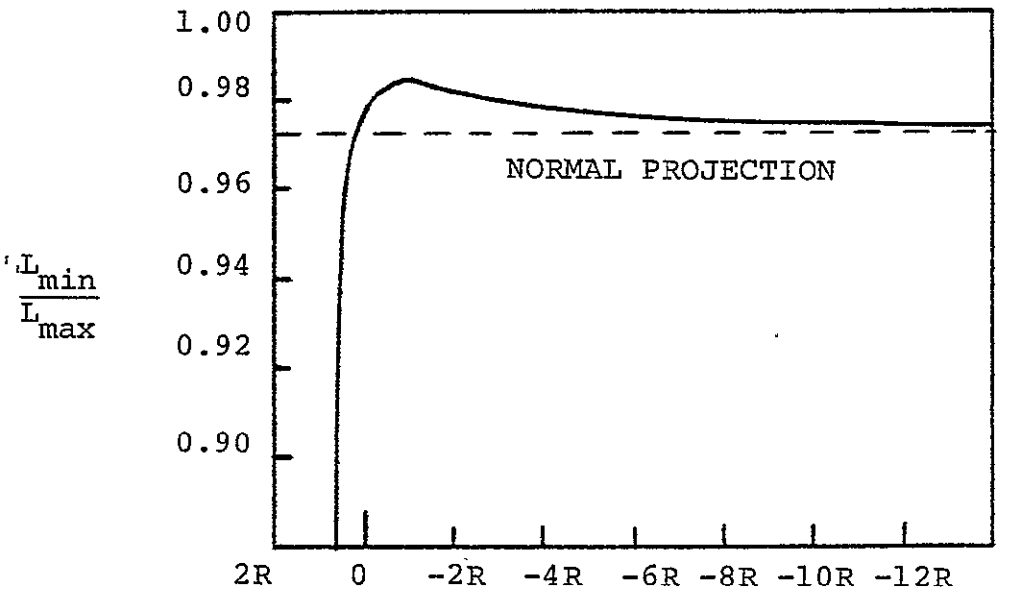

FIG. 25. VARIATION OF $\frac{L_{min}}{L_{max}}$ FOR A PARABOLOIDAL DISH AS A FUNCTION OF PROJECTION CENTER (FOD = 1.0, n=6, N=10, D=100m)

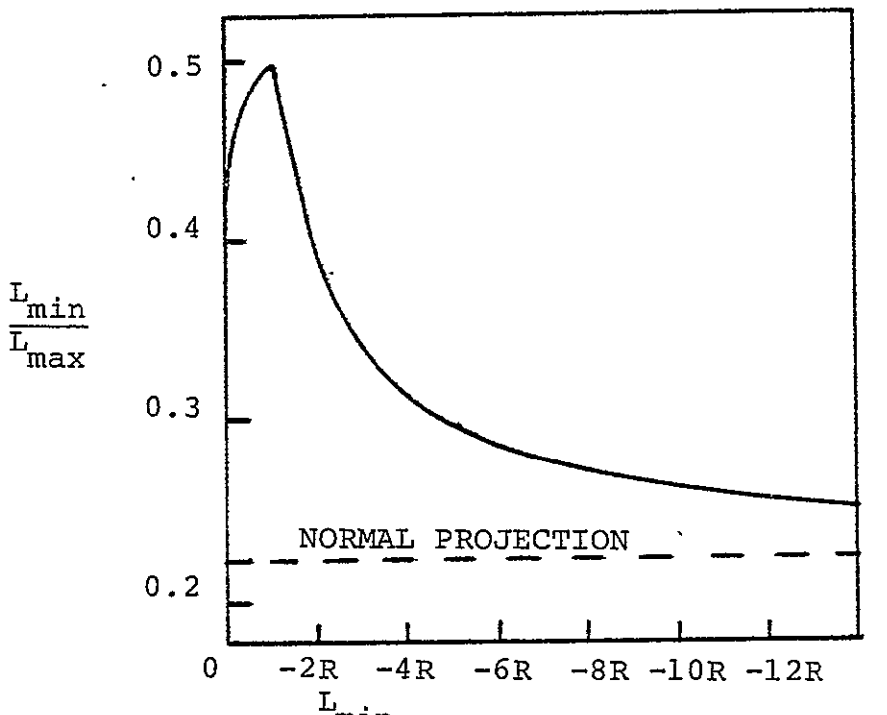

FIG. 26. VARIATION OF $\frac{L_{min}}{L_{max}}$ FOR A SPHERICAL DISH AS A FUNCTION OF PROJECTION CENTER (FOD=0.25, n=6, N=10, D=100m)

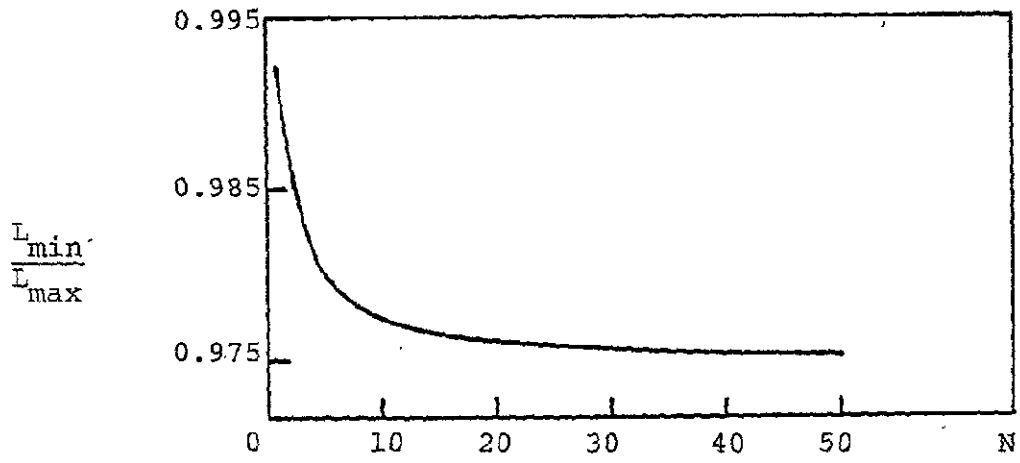

FIG. 27. VARIATION OF $\frac{L_{min}}{L_{max}}$ WITH FREQUENCY FOR A PARABOLOIDAL DISH (FOD=1., n=6, D=100m, CENTER OF PROJECTION (0,0,0))

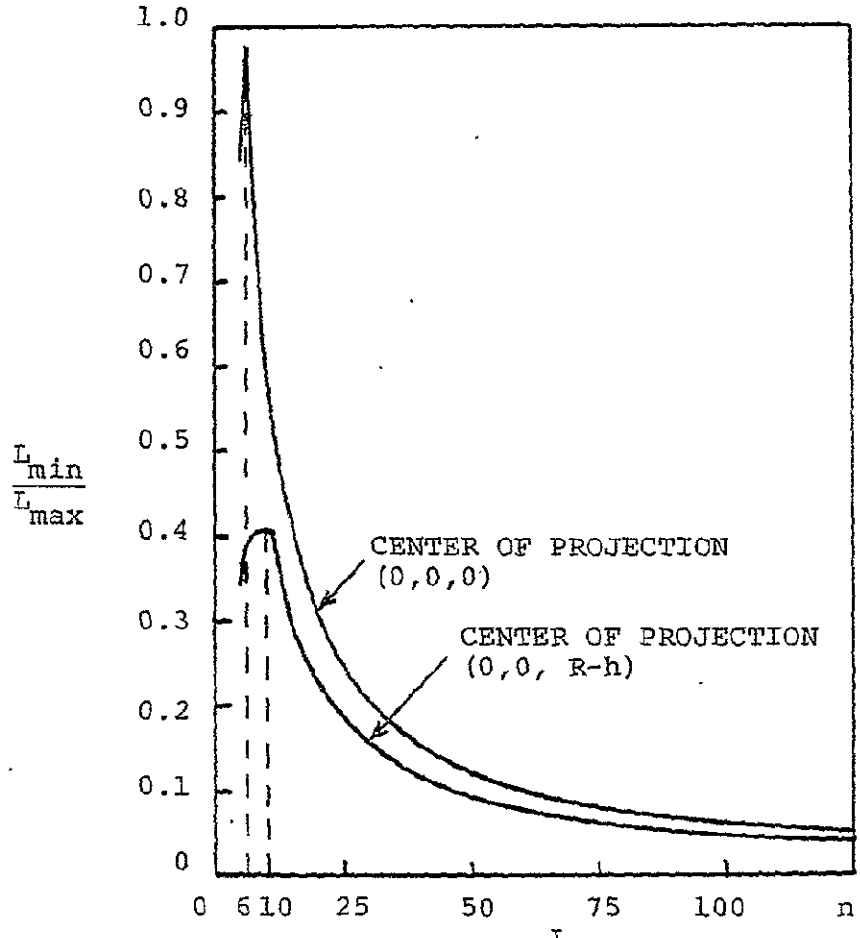

FIG. 28. VARIATION OF $\frac{L_{min}}{L_{max}}$ OF A PARABOLOIDAL DISH WITH n (FOD=1., D=100m, N=10)

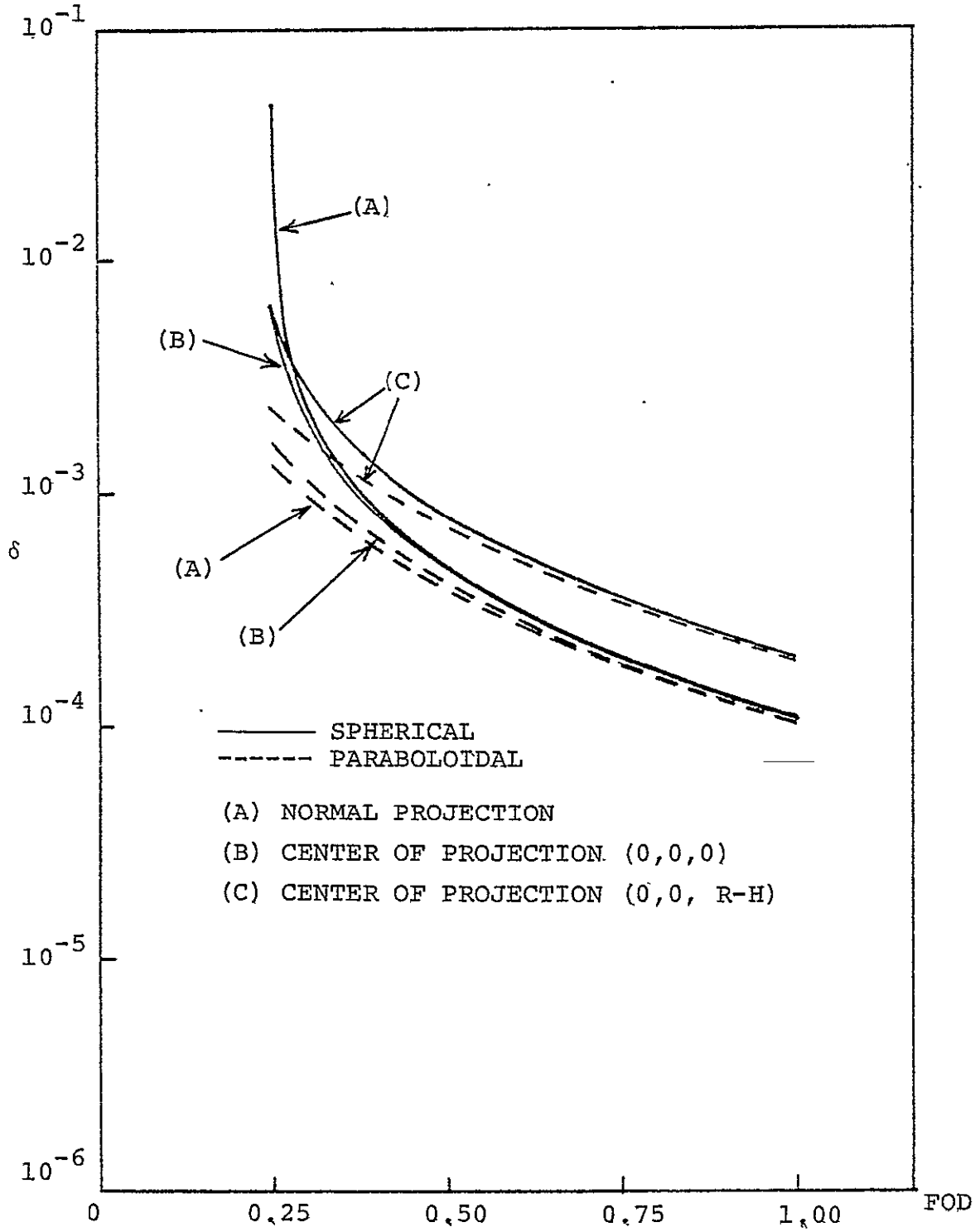

FIG. 29. VARIATION OF NORMALIZED DEVIATION, δ, WITH FOD FOR A VARIETY OF PROJECTION CENTERS (n=6, N=10, D=100m)

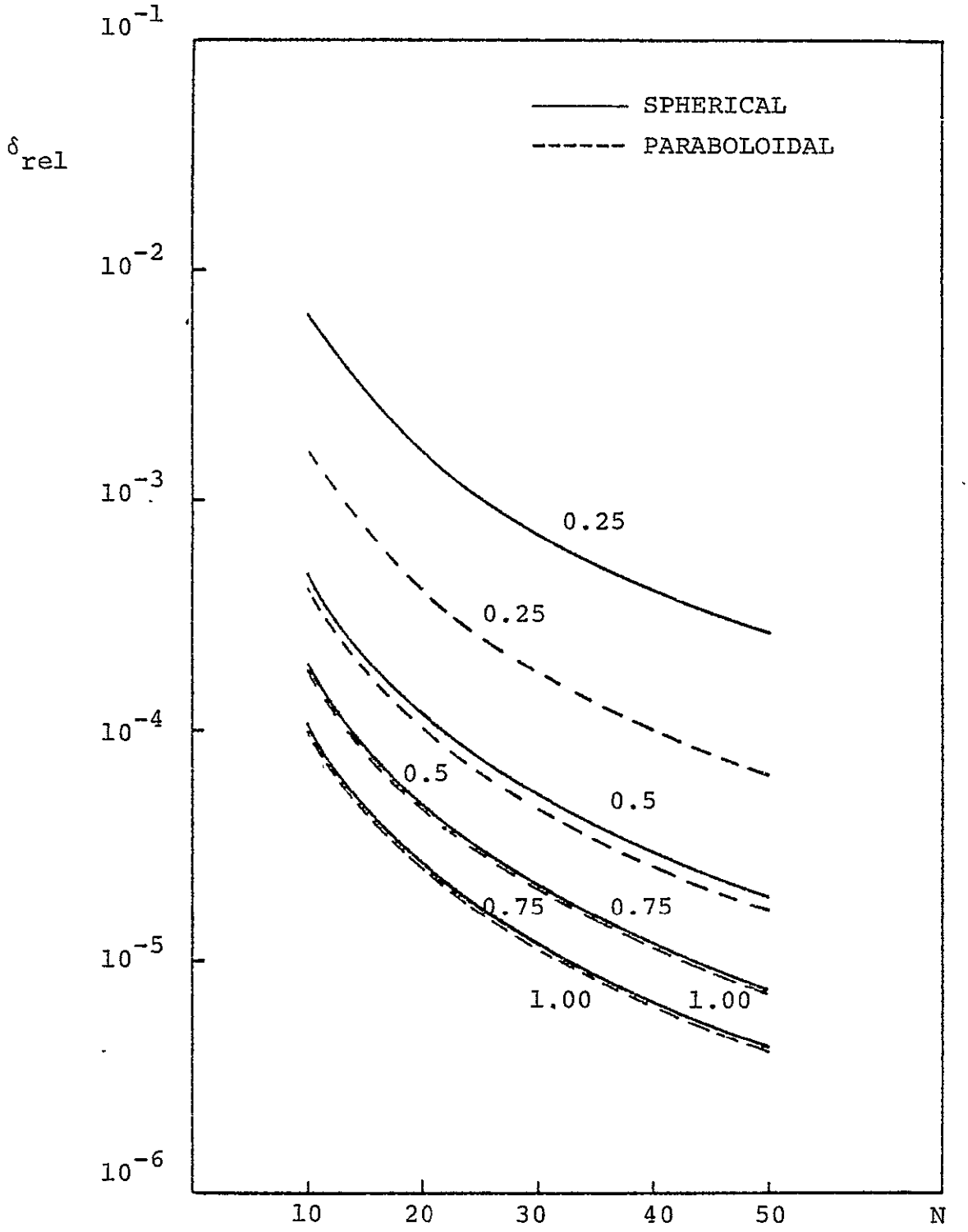

FIG. 30. VARIATION OF δ WITH N FOR A VARIETY OF FOD VALUES (n=6, D=100m, AND CENTER OF PROJECTION (0,0,0))

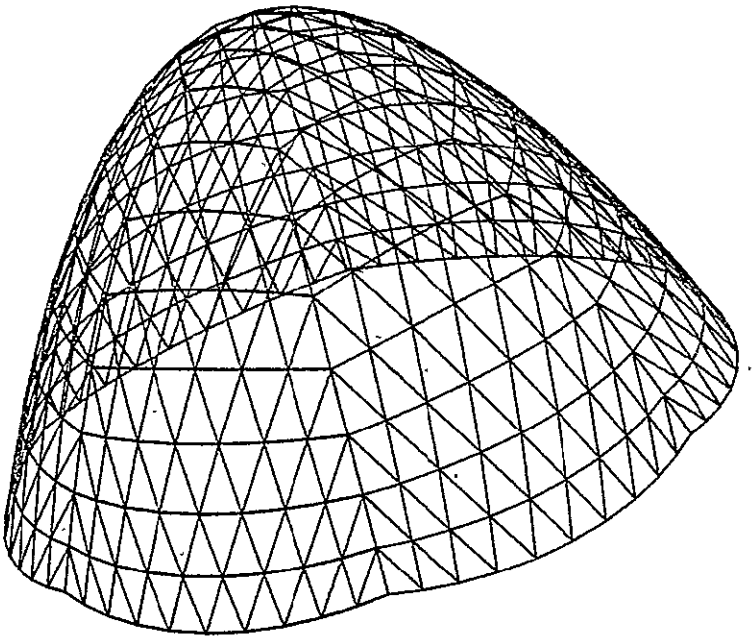

(a) FOD = 0.1

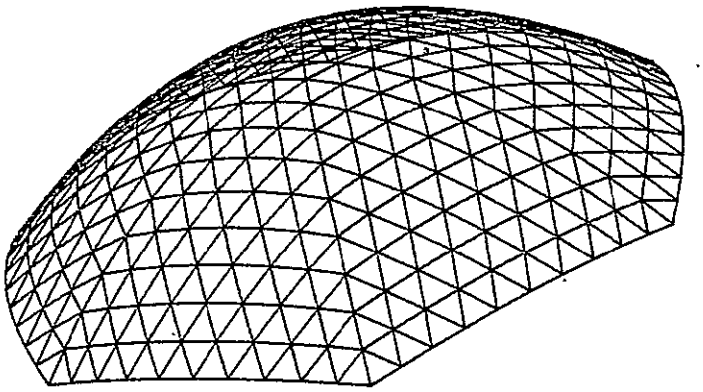

(b) FOD = 0.25

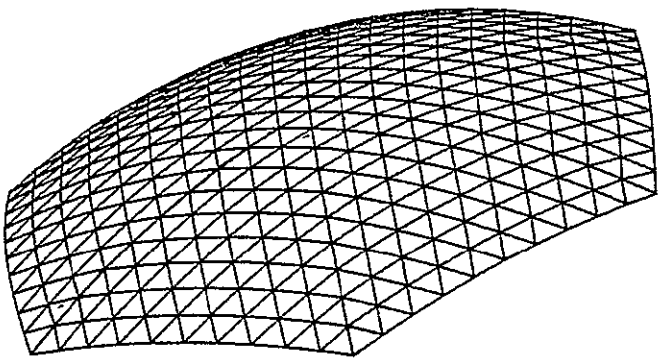

(c) FOD = 0.5

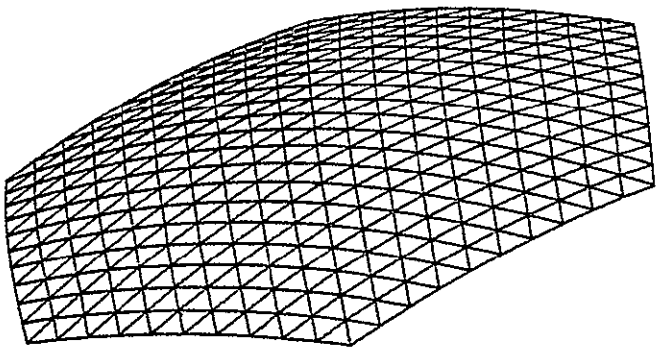

(d) FOD = 0.75

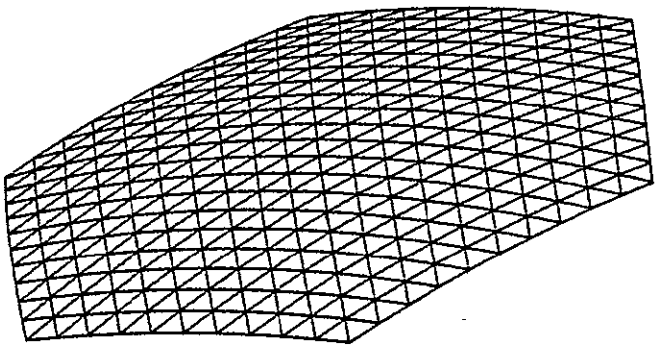

(e) FOD = 1.0

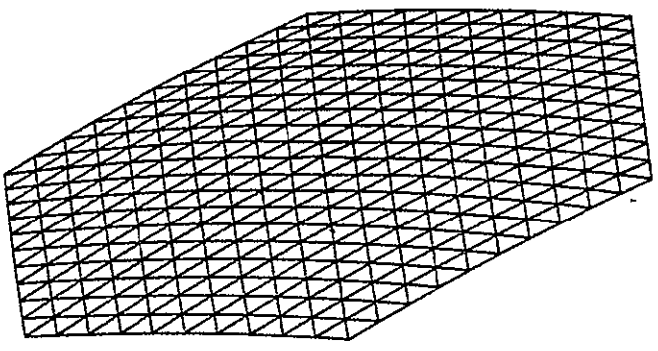

(f) FOD = 2.0

FIG. (31a-f) PLOTS OF PARABOLOIDAL DISHES FOR A VARIETY OF FOD (n=6, N=10, D=100m, CENTER OF PROJECTION (0,0,0), $(\alpha_1,\alpha_1,\alpha_3) = (60^{\circ}, 30^{\circ}, 30^{\circ})$

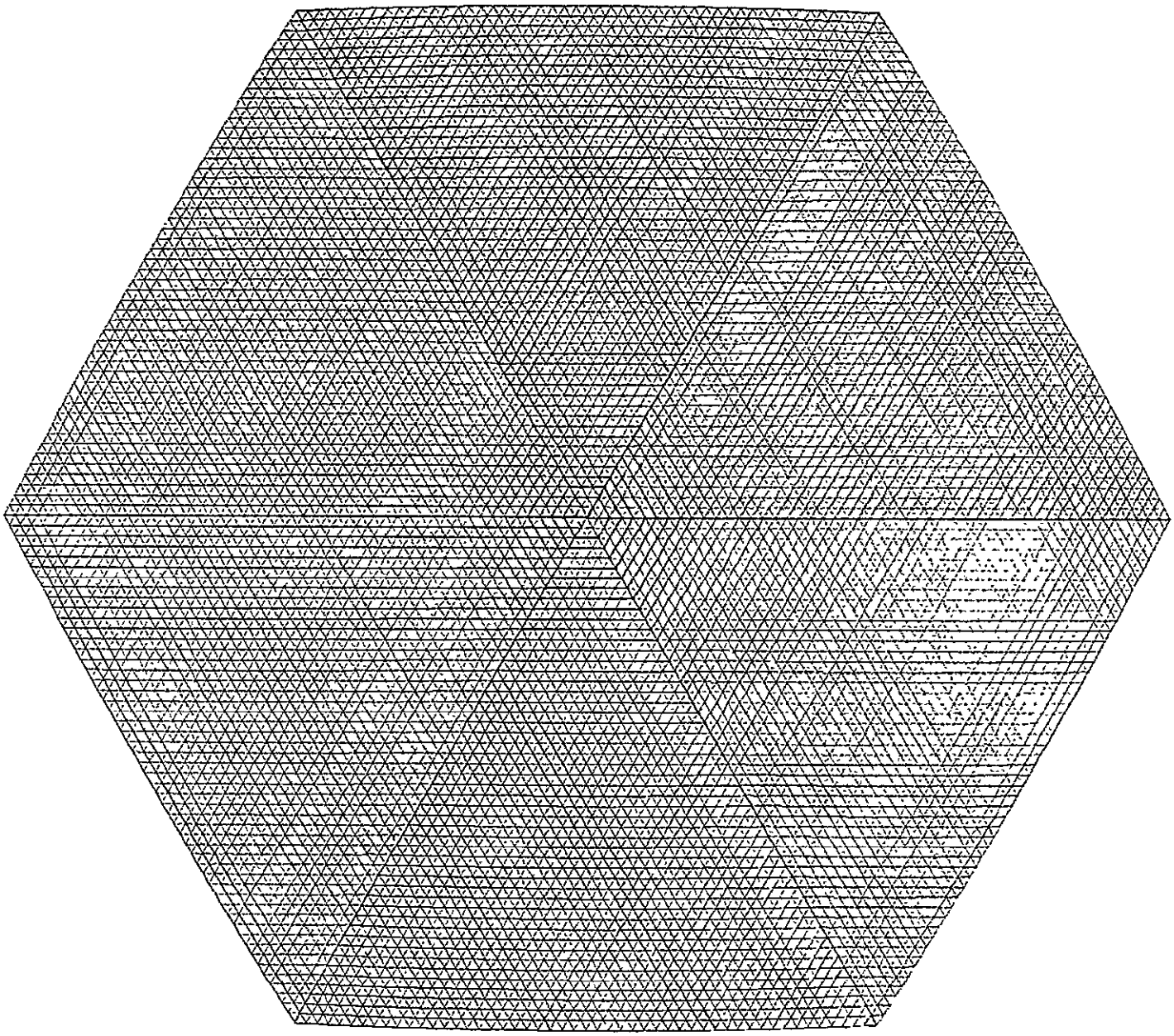

FIG. 32a. VERTICAL VIEW OF A SPHERICAL DISH (n=b, N=50, D=725m, FOD = .793 AND CENTER OF PROJECTION (0,0,0))

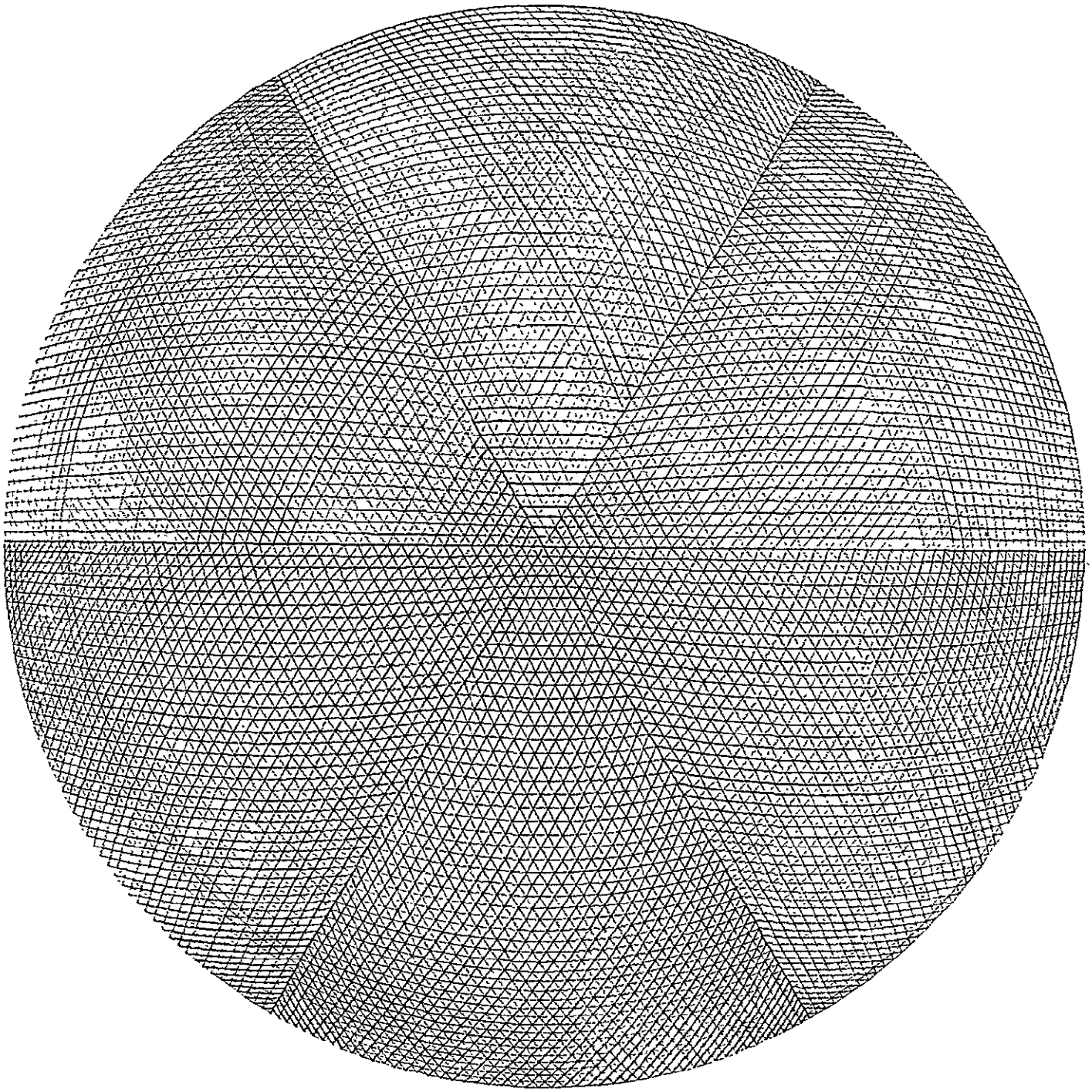

FIG. 32b. SAME AS THAT OF FIG. 32a WITH CENTER OF PROJECTION (0,0, R-H)

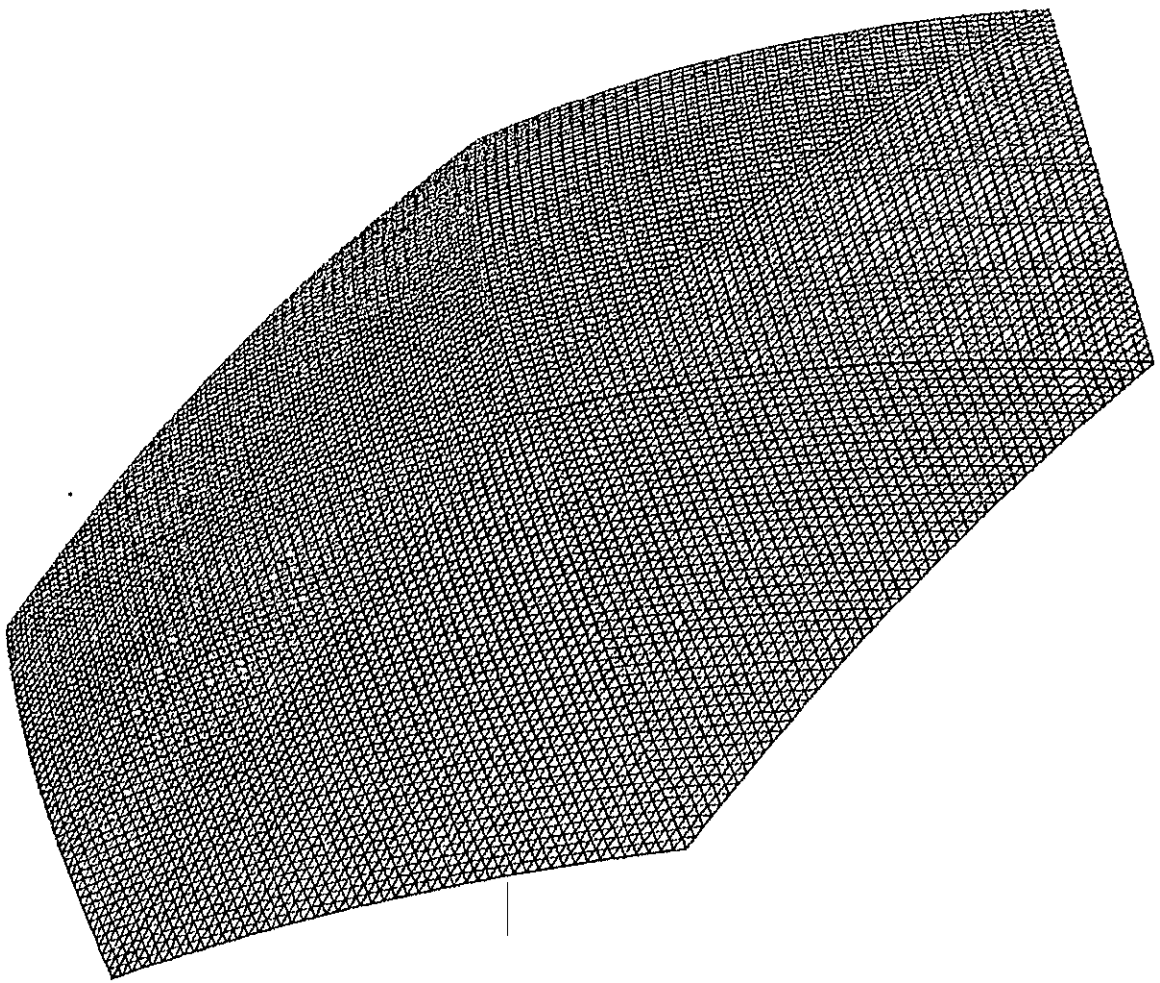

FIG. 32c. SAME AS FIG. 32a WITH VIEW GIVEN BY $(\alpha_1, \alpha_2, \alpha_3) = (45^{\circ}, 45^{\circ}, 45^{\circ})$.

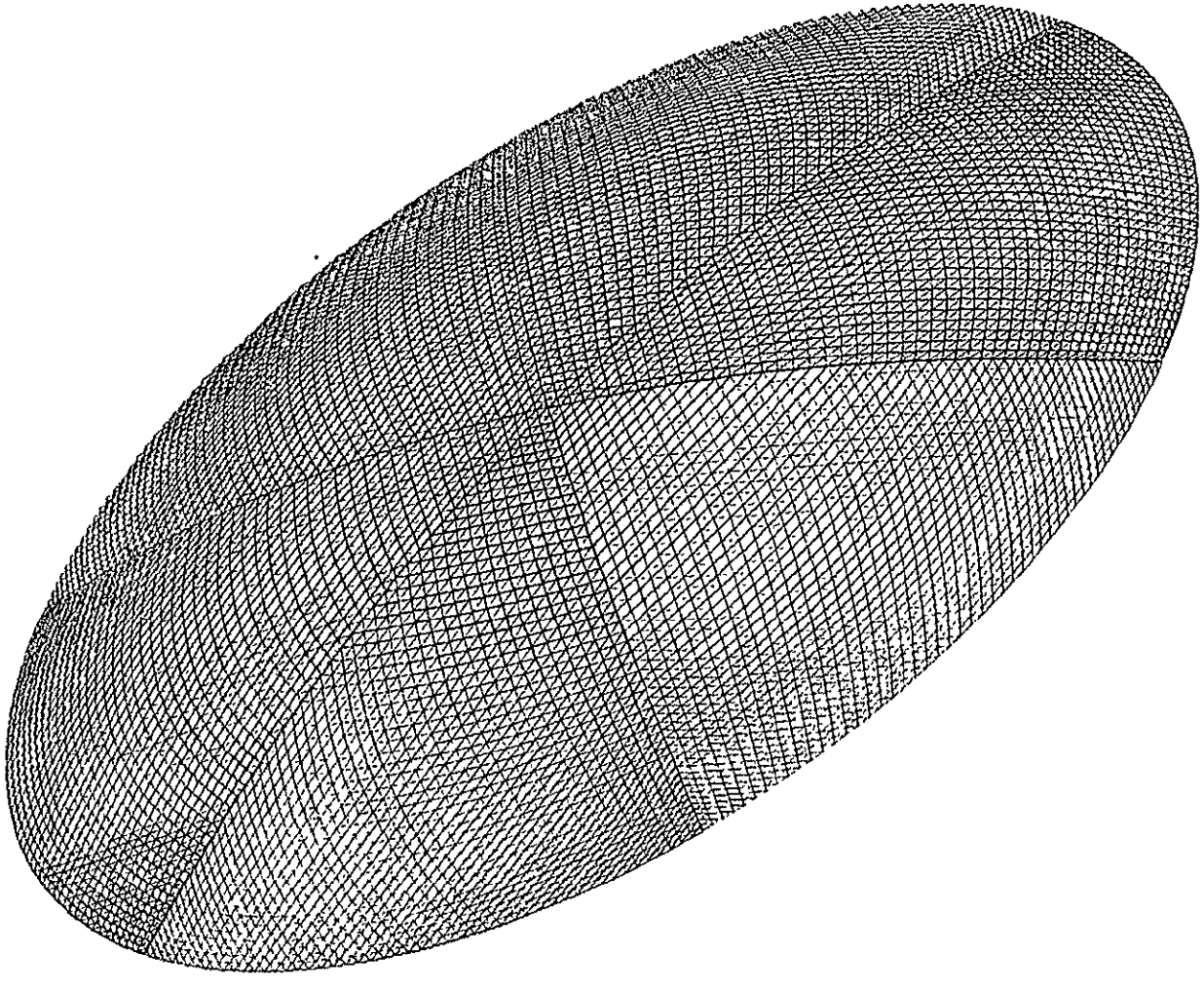

FIG. 32d. SAME AS FIG. 32b WITH VIEW GIVEN BY $(\alpha_1, \alpha_1, \alpha_3) = (45^{\circ}, 45^{\circ}, 45^{\circ})$

REFERENCES

1. Hagler, T., "Building Large Structures in Space", Astronautics and Aeronautics, May 1976, pp. 56-61.

2. Culbertson, P.E., and Bold, P., "Opening a New Era in Space", Astronautics and Aeronautics, April 1977, pp. 20-25.

3. Daros, C.J., Freitag, R., and Kline, R., "Toward Large Space System", Astronautics and Aeronautics, May 1977, pp. 22-30.

4. Woodcock, G.R., "Solar Satellites, Space Key to Our Power Future", Astronautic and Aeronautics, July/August 1977, pp. 30-43.

5. Davis, R.M., Editor, Space Structures, A Study of Methods and Developments in Three-Dimensional Construction Resulting from the International Conference on Space Structures, University of Surrey, September 1966, John Wiley and Sons, Inc.

6. Noor, A.K., Green, W.H., and Anderson, M.S., "Continuum Models for Static and Dynamic Analysis of Repetitive Lattice", AIAA/ASME/SAE 18th Structures, Structural Dynamics and Materials Conference, (1977).

7. Mikulas, M.M., Jr., Bush, H.G., and Card, M.F., "Structural Stiffness, Strength and Dynamic Charactertistics of Large Tetrahedral Space Truss Structures", NASA TMX 74001, 1977.

8. Nayfeh, A.H., and Hefzy, M.S., "Continuum Modeling of Three-Dimensional Truss Like Space Structures", NASA CR No. 145248, September 1977.

9. Nayfeh, A.H., and Hefzy, M.S., "Continuum Modeling of Two-Dimensional Plate-Like Discrete Structures", In preparation and will be submitted for possible publication as a NASA Langley CR.

10. Clinton, J.D., "Advanced Structural Geometry Studies, Part I - Polyhedral Subdivision Concepts for Structural Applications", NASA CR-1734, September, 1971.

11. Lauchner, J., Fuller, R.B., Clinton, J., Mabee, M., Moeller, R. and Flood, R., "Structure Design Concepts for Future Space Missions", NASA CR-101577, 1968.

APPENDIX A

A computer program is written so that we can graphically illustrate the cap's discrete surfaces for any three-dimensional orientation. Due to the rotational symmetry about the z-axis we draw all of the cap once we know how to draw one of the pyramid's face triangles.

Let $(X^{(1)}, Y^{(1)}, Z^{(1)})$ be the coordinates of a point in the first triangle face of figure A1. The coordinates of the corresponding points on the adjacent faces (counterclockwise) will be $(X^{(2)}, Y^{(2)}, Z^{(2)})$, $(X^{(3)}, Y^{(3)}, Z^{(3)})$, ---- $(X^{(n)}, Y^{(n)}, Z^{(n)})$, respectively, (see fig. A1). Notice also that $Z^{(1)} = Z^{(2)} = Z^{(3)} = \ldots Z^{(n)}$. Let us use polar coordinates; the the point $(X^{(m)}, Y^{(m)}, Z^{(m)})$ can be written in polar form (while suppressing the z-coordinate) as

$$X^{(m)} + iY^{(m)} = re^{i\theta}e^{i(m-1)\phi} \tag{A1}$$

where $m = 1,2,3, \ldots n$

$$\phi = \frac{2\pi}{n} \tag{A2}$$

Now suppose that we introduce a new system of axes $\bar{X}$, $\bar{Y}$ and $\bar{Z}$ (see fig. A2) which is fixed in the body of the cap but moves with it. Also suppose we give to the cap any orientation with respect to the fixed system of axes X, Y and Z. We must choose the origin, $\bar{o}$, of the system $\bar{X}$, $\bar{Y}$ and $\bar{Z}$ to be the same as the origin, o of the system X, Y and Z By projecting the cap in the (X-Y) plane or the (Y-Z) plane, we obtain a view of the cap in a required orientation. The question is knowing the values of $\bar{X}_i$, $\bar{Y}_i$ and $\bar{Z}_i$ for a specific point what would be the corresponding values of X_i, Y_i and Z_i. This can be done by referring to the Eulers angles. First let us fix our system of axes in space X,Y and Z. Then we start our orientation process by letting ($\bar{X}$, $\bar{Y}$ and $\bar{Z}$) which are fixed

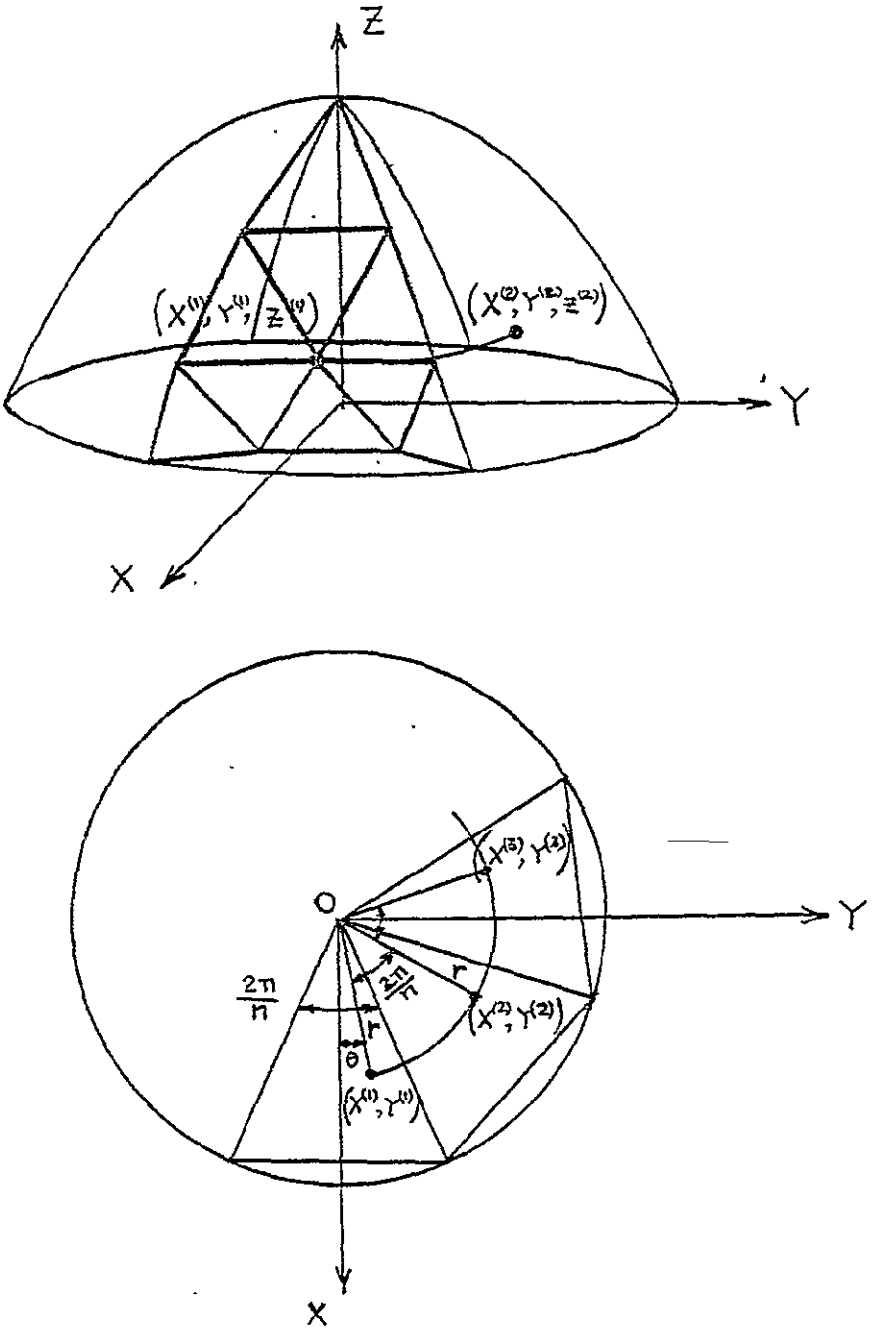

FIG. A1. LOCATIONS OF POINTS ON THE SOLID SURFACE

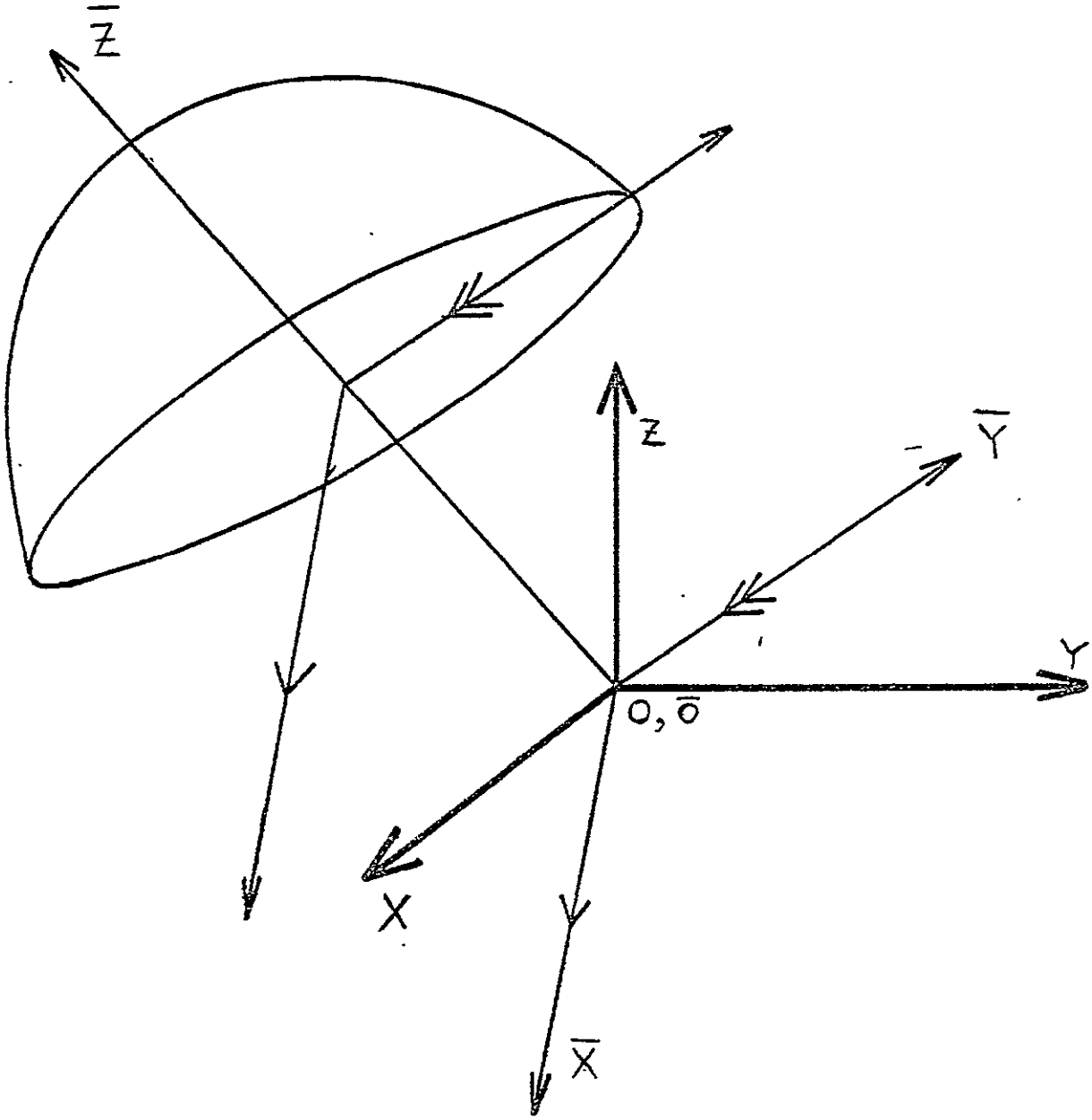

FIG. A2. COORDINATE TRANSFORMATION

in the body of the cap coincide with the fixed system X, Y and Z. At this stage, we start to rotate the body around the $\bar{Z}$ axes with an angle α_1. (see figure (A3)). To make it easier to illustrate let us use the notation $\bar{n}_i$ which represent unit vectors along the direction of the fixed axes in the body before rotation and let $\bar{n}_i^{(1)}$ represent unit vectors along the direction of the axes after this first rotation. The relation between these unit vectors are given by

$$\begin{bmatrix} \bar{n}_1 \\ \bar{n}_2 \\ \bar{n}_3 \end{bmatrix} = \begin{bmatrix} \cos\alpha_1 & -\sin\alpha_1 & 0 \\ \sin\alpha_1 & \cos\alpha_1 & 0 \\ 0 & 0 & 1 \end{bmatrix} \begin{bmatrix} \bar{n}_1^{(1)} \\ \bar{n}_2^{(1)} \\ \bar{n}_3^{(1)} \end{bmatrix} \tag{A3}$$

Now, let us rotate the body at the new position of $\bar{X}$, i.e. around $\bar{n}_1^{(1)}$, with an angle α_2 to obtain a new set of axes $\bar{n}_i^{(2)}$ related to the preceding by

$$\begin{bmatrix} \bar{n}_1^{(1)} \\ \bar{n}_2^{(1)} \\ \bar{n}_3^{(1)} \end{bmatrix} = \begin{bmatrix} 1 & 0 & 0 \\ 0 & \cos\alpha_2 & -\sin\alpha_2 \\ 0 & \sin\alpha_2 & \cos\alpha_2 \end{bmatrix} \begin{bmatrix} \bar{n}_1^{(2)} \\ \bar{n}_2^{(2)} \\ \bar{n}_3^{(2)} \end{bmatrix} \tag{A4}$$

To end our process of orientation, let us rotate the body about the new position of $\bar{Z}$, i.e. around $\bar{n}_3^{(2)}$, with an angle α_3 to obtain the final set of axes $\bar{n}_i^{(3)}$. One notices that this is the set of axes $\bar{X}^B$, $\bar{Y}^B$ and $\bar{Z}^B$ which is fixed in the cap and one also notices that the coordinates of any point on the cap's surface with respect to that set of axes are known and related to the preceding by

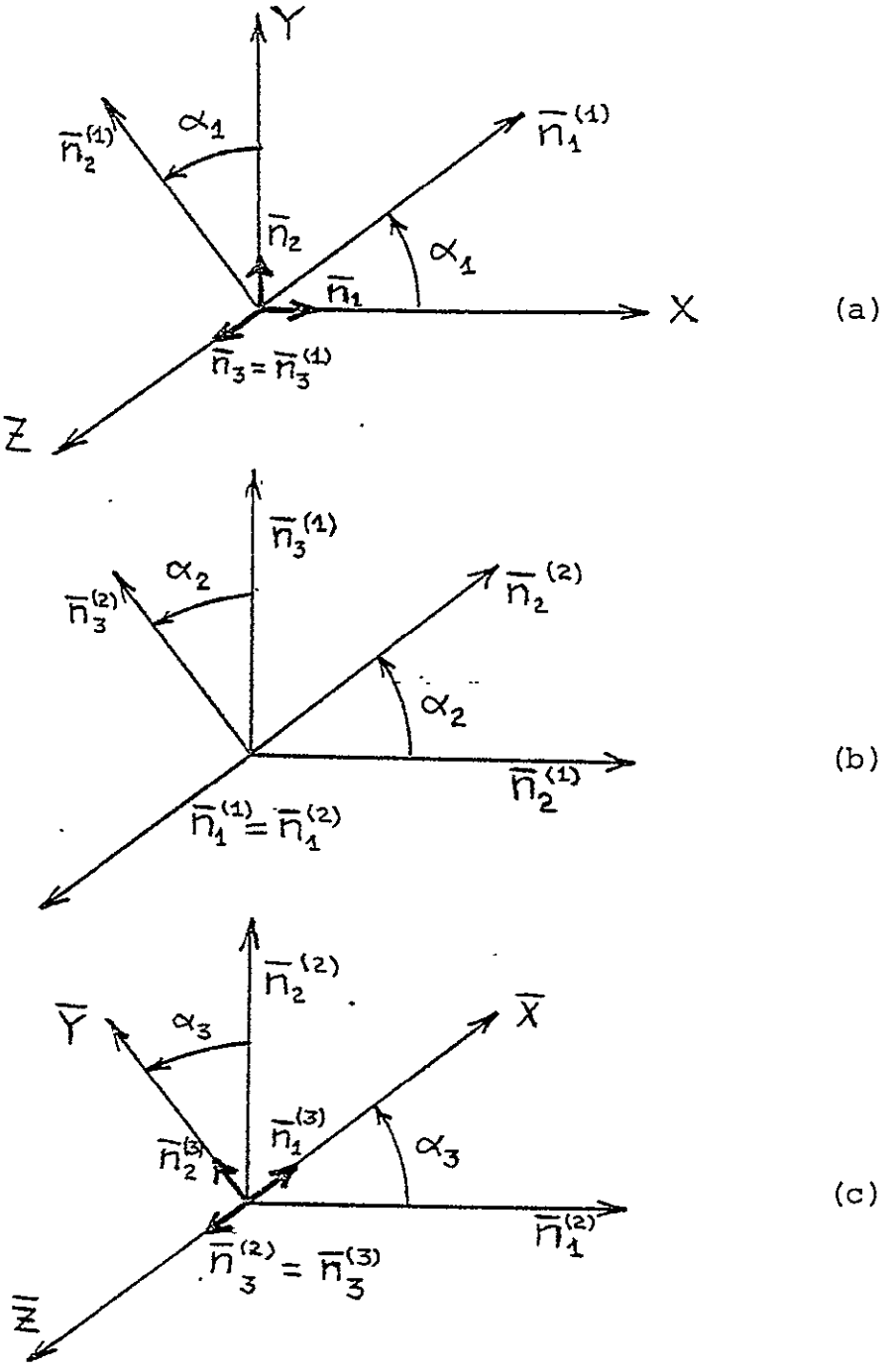

FIG. A3. EULER'S ANGLES

$$\begin{bmatrix} \bar{n}_1^{(2)} \\ \bar{n}_2^{(2)} \\ \bar{n}_3^{(2)} \end{bmatrix} = \begin{bmatrix} \cos\alpha_3 & -\sin\alpha_3 & 0 \\ \sin\alpha_3 & \cos\alpha_3 & 0 \\ 0 & 0 & 1 \end{bmatrix} \begin{bmatrix} \bar{n}_1^{(3)} \\ \bar{n}_2^{(3)} \\ \bar{n}_3^{(3)} \end{bmatrix} \tag{A5}$$

So, accordingly we finally obtain the relation

$$\begin{bmatrix} X_i \\ Y_i \\ Z_i \end{bmatrix} = \begin{bmatrix} \cos\alpha_1 & -\sin\alpha_1 & 0 \\ \sin\alpha_1 & \cos\alpha_1 & 0 \\ 0 & 0 & 1 \end{bmatrix} \begin{bmatrix} 1 & 0 & 0 \\ 0 & \cos\alpha_2 & -\sin\alpha_2 \\ 0 & \sin\alpha_2 & \cos\alpha_2 \end{bmatrix} \begin{bmatrix} \cos\alpha_3 & -\sin\alpha_3 & 0 \\ \sin\alpha_3 & \cos\alpha_3 & 0 \\ 0 & 0 & 1 \end{bmatrix} \begin{bmatrix} \bar{X}_i \\ \bar{Y}_i \\ \bar{Z}_i \end{bmatrix} \tag{A6}$$

or equivalently is

$$\begin{aligned} X_i = {} & (\cos\alpha_1\cos\alpha_3 - \sin\alpha_1\cos\alpha_2\sin\alpha_3)\bar{X}_i \\ & + (-\cos\alpha_1\sin\alpha_3 - \sin\alpha_1\cos\alpha_2\cos\alpha_3)\bar{Y}_i \\ & + (\sin\alpha_1\sin\alpha_2)\bar{Z}_i \end{aligned} \tag{A7}$$

$$\begin{aligned} Y_i = {} & (\sin\alpha_1\cos\alpha_3 + \cos\alpha_1\cos\alpha_2\sin\alpha_3)\bar{X}_i \\ & + (-\sin\alpha_1\sin\alpha_3 + \cos\alpha_1\cos\alpha_2\cos\alpha_3)\bar{Y}_i \\ & + (-\cos\alpha_1\sin\alpha_2)\bar{Z}_i \end{aligned} \tag{A8}$$

$$Z_i = (\sin\alpha_2\sin\alpha_3)\bar{X}_i + (\sin\alpha_2\cos\alpha_3)\bar{Y}_i + \cos\alpha_2\bar{Z}_i. \tag{A9}$$

So, for different values for the angles α_1, α_2 and α_3, one can obtain different view from different angles to the cap. Some results of our plottings are illustrated in figures 31 and 32, for both spherical and paraboloidal caps.